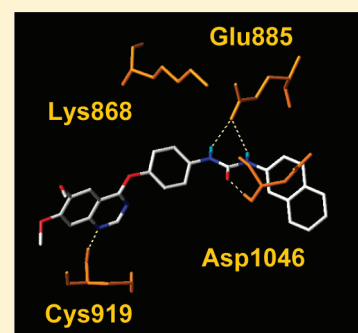


Synthesis and Structure–Activity Relationships of
(Aryloxy)quinazoline Ureas as Novel, Potent, and Selective Vascular
Endothelial Growth Factor Receptor-2 InhibitorsAntonio Garofalo,^{†,‡} Amaury Farce,^{*,†,§} Séverine Ravez,^{†,‡} Amélie Lemoine,^{†,‡} Perrine Six,^{†,‡}
Philippe Chavatte,^{†,§} Laurence Goossens,^{†,‡} and Patrick Depreux^{†,‡}[†]Univ. Lille Nord de France, F-59000 Lille, France[‡]Institut de Chimie Pharmaceutique Albert Lespagnol (ICPAL) and [§]Laboratoire de Chimie Thérapeutique, UFR de Pharmacie, Univ. Lille 2 Droit et Santé (UDSL), EA4481, F-59006 Lille, France

ABSTRACT: In our continuing search for medicinal agents to treat proliferative diseases, quinazoline derivatives were synthesized and evaluated pharmacologically as epithelial growth factor receptor and vascular endothelial growth factor receptor 2 (VEGFR-2) tyrosine kinase inhibitors. A quantitative structure–activity relationship analysis was conducted to rationalize the structure–activity relationship and to predict how similar the inhibitor-binding profiles of two protein kinases are likely to be on the basis of the docking of lead compounds into the ATP-binding site. This model was used to direct the synthesis of new compounds. A series of *N*-(aromatic)-*N'*-{4-[(6,7-dimethoxyquinazolin-4-yl)oxy]-phenyl}urea were identified as potent and selective inhibitors of the tyrosine kinase activity of VEGFR-2 (fetal liver kinase 1, kinase insert domain-containing receptor). An efficient route was developed that enabled the synthesis of a wide variety of analogues with substitution on several positions of the template. Substitution of diarylurea, competitive with ATP, afforded several analogues with low nanomolar inhibition of enzymatic activity of VEGFR-2. In this paper, we describe the synthesis, structure–activity relationships, and pharmacological characterization of the series.



■ INTRODUCTION

Protein kinases constitute one of the largest protein families and are implicated in many diseases by alteration in their kinase-mediated signaling pathways, such as cancer, diabetes, and inflammatory disorders.^{1–3} Protein kinases play important roles in regulating most of the cellular functions (proliferation, cell cycle, cell metabolism, survival, apoptosis, DNA damage/repair, ...) by multiple pathways, which makes them attractive as drug targets.^{4–7} In recent years, angiogenesis has become an attractive therapeutic target.⁸ Pathological angiogenesis has been associated with a variety of diseases, including diabetes retinopathy, psoriasis, rheumatoid arthritis, and cancer.⁹ This pathology is an essential series of molecular events that occur during the formation of new blood vessels from the endothelium of preexisting vasculature and plays a vital role in tumor growth. Solid tumors cannot grow beyond a critical size until they develop new collateral blood vessels to provide oxygen and nutrients, elimination of waste materials generated from tumor metabolism, and cell dissemination leading to metastasis to other organs.^{10–12}

Among the many proangiogenic factors, vascular endothelial growth factor (VEGF) has been identified as the most common regulator of tumor angiogenesis, including vascular permeability, endothelial cell activation, proliferation, and migration.^{13–16} Crucial steps in angiogenesis are mediated through a specific VEGF receptor, the kinase insert domain-containing receptor (KDR; or vascular endothelial growth factor 2 (VEGFR-2)).

This receptor tyrosine kinase (RTK) has been shown to be an important mediator of signal transduction in cells.^{17–21} These membrane molecules characteristically consist of an extracellular ligand-binding domain connected through a segment in the plasma membrane to an intracellular tyrosine kinase domain.^{22,23} Binding of the ligand to the receptor results in receptor dimerization and stimulation of the receptor-associated tyrosine kinase activity, which leads to phosphorylation of tyrosine residues and initiates a signaling cascade leading to a variety of cellular responses.^{24–26}

Throughout the past two decades, inhibition of VEGF activity or VEGFR-2 kinase has been shown to inhibit angiogenesis, tumor progression, and dissemination in a number of preclinical and clinical studies.^{27–34} From examples, the use of the neutralizing monoclonal antibody against VEGF, bevacizumab,^{32,33} has demonstrated a prolonged survival in colorectal cancer patients. In addition, small-molecule tyrosine kinase inhibitors of KDR, such as sorafenib (a dual Raf–KDR inhibitor)^{34,35} and sunitinib (a multitargeted kinase),³⁶ have been approved for treatment of cancers (Figure 1). Up to now, there has been a lot of research focusing on the development of novel inhibitors of KDR as vandetanib (ZD6474), orally bioavailable in phase III, considered to be a dual tyrosine kinase inhibitor targeting EGFR and VEGFR-2.^{37–39}

Received: October 7, 2011

Published: January 9, 2012

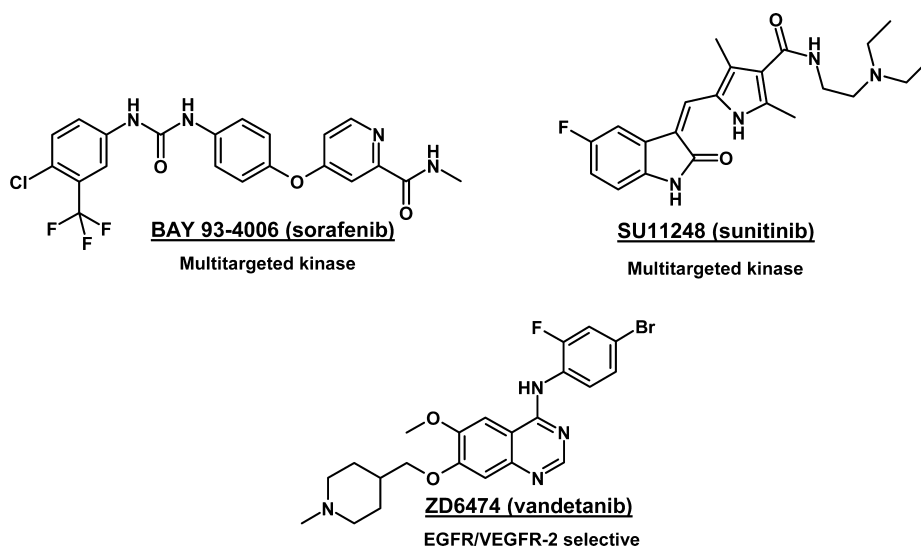


Figure 1. Examples of tyrosine kinase inhibitors undergoing clinical trials or marketed.

Often, the fact that the biological targets belong to the same family of receptors raises the problem of selectivity. Special efforts to design multiple activating drugs can be successful using computational methods to support biochemical studies and to design selective ligands for receptor subtypes.

In the present work, molecular modeling studies of these novel VEGFR-2 inhibitors were performed using a three-dimensional quantitative structure–activity relationship (3D QSAR) and docking approach. 3D QSAR methods, such as comparative molecular field analyses (CoMFA) and comparative molecular similarity index analyses (CoMSIA), were applied to these inhibitors to gain insight into how steric, electrostatic, hydrophobic, and hydrogen-bonding interactions influence their activities. In our research for selective KDR kinase inhibitors, we have recently disclosed the structure–activity relationships (SARs) of quinazoline derivatives (Figure 2)

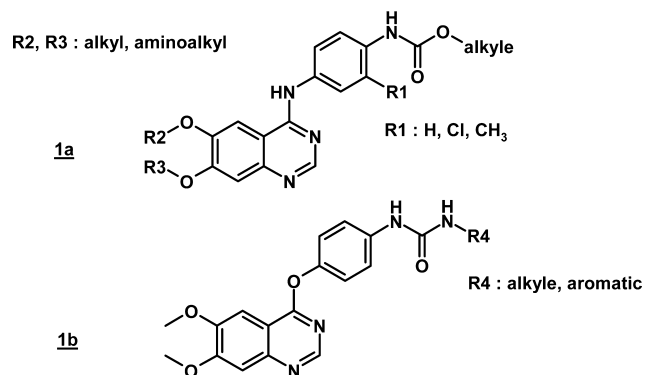


Figure 2. General structures of synthesized carbamic acid esters **1a** and aryloxy derivatives **1b**.^{40–42}

as anticancer drugs.^{41,42} Herein, we describe the SAR and pharmacology of a novel series of quinazoline carbamic acid esters, dual EGFR/VEGFR-2 kinase inhibitors,⁴¹ and of (aryloxy)-quinazoline ureas, selective VEGFR-2 kinase inhibitors.⁴²

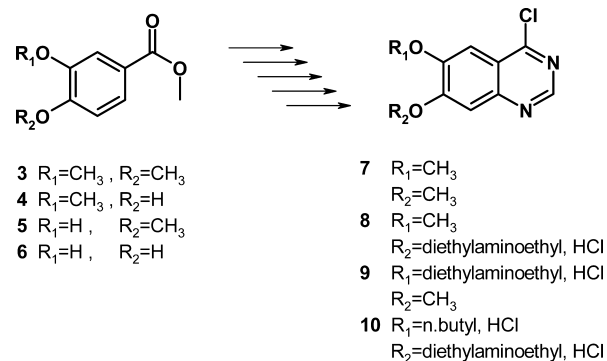
In an effort to further develop this series, a QSAR model has been derived from this activity in a two-step process. First, the docking of the most active compound of the two families of molecules has been realized to achieve a putative bioactive

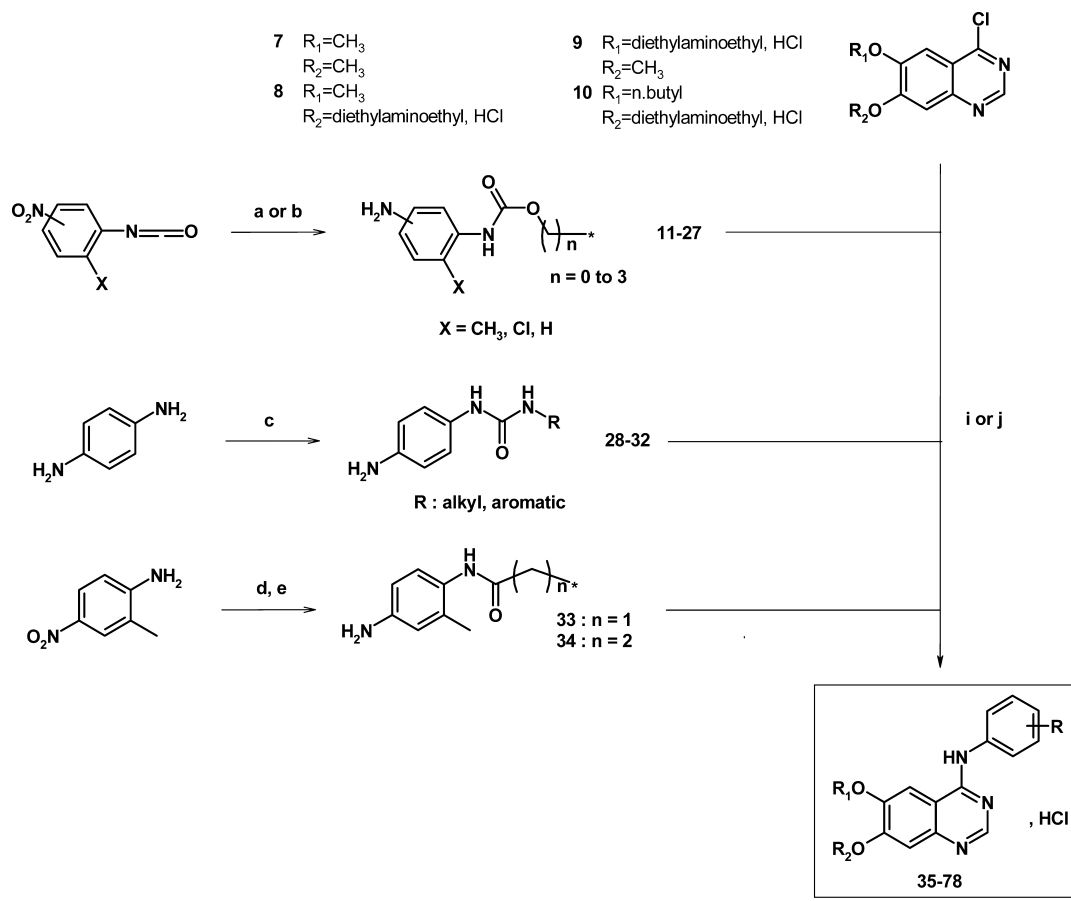
conformation. Second, 3D QSAR models employing the CoMFA and CoMSIA methods have been elaborated on the basis of an alignment of the compounds on the putative bioactive conformation of the two reference molecules. The excellent agreement between the docking and the QSAR fields indicates that the binding mode hypothesis is most probably fairly close to the biological binding mode, therefore offering a relevant basis for proposing improvements for the further development of the series. The second major interest of this study is the predictive power of the models, more than their insights into the structural modifications that would enhance the activity of the series, which is too homogeneous to provide an efficient basis for suggesting new scaffolds. This predictive power has been validated on external test sets and further proved on newly designed selective VEGFR-2 inhibitors. These compounds have been synthesized and evaluated in our whole cell assay by measuring the inhibition of VEGFR-2 and EGFR to provide their selectivity and antiproliferative activity toward prostate (PC3), breast (MCF-7), and colon (HT-29) cancer cells.

CHEMISTRY

In our research to discover a new anticancer drug, we designed and evaluated pharmacologically 200 compounds as potent kinase inhibitors. Sixty of these compounds were used for this study. They were prepared via a generalized route outlined in Schemes 1–3.

Scheme 1. Synthesis of Quinazoline Intermediates



Scheme 2^a

^aReagents and conditions: (a) Raney nickel, H_2 , CH_2Cl_2 , ROH (80–90%); (b) Raney nickel, H_2 , CH_2Cl_2/THF (1/1), ROH (80–90%); (c) isocyanate, $CHCl_3$ (70–80%); (d) $RCOCl$, triethylamine, THF, 0–20 °C (70–85%); (e) Raney nickel, H_2 , MeOH (80–90%); (i) anilines, 2-propanol, reflux (60–80%); (j) anilines, NaH, DMF, 50 °C (25–40%).

The synthesis and spectroscopic data of 4-chloroquinazoline derivatives 7–10 have been reported (Scheme 1).^{40–42}

The synthesis of (aminophenyl)carbamic acid esters 11–27 was performed by a one-pot reduction procedure of the corresponding nitrophenyl isocyanate in the presence of various alcohols in a CH_2Cl_2/THF mixture.⁴⁶ Condensation of 1,4-phenylenediamine and the corresponding isocyanate in $CHCl_3$ afforded the desired ureas 28–32 in high yields and short reaction times.⁴⁷ Amide analogues 33 and 34 were prepared from 2-methyl-4-nitroaniline according to a two-step procedure: acetylation from chloride derivatives and reduction under a hydrogen atmosphere using Raney nickel as the catalyst.⁴¹ Target compounds 35–78 were obtained by nucleophilic substitution with previously synthesized anilines 11–34 either in 2-propanol or in DMF in the presence of sodium hydride (40–60%). The desired anilinoquinazolines 35–78 were isolated as hydrochloride salts (Scheme 2).

In Scheme 3, 4-chloro-6,7-dimethoxyquinazoline (7) was used to prepare the aryloxy derivatives 79–93.⁴⁸ Heating at 150 °C in DMSO of quinazoline 7 with phenol derivatives gave products 79–81 in good yields. Amidification or condensation with aniline intermediates 94 and 95 afforded carbamic acid esters 82 and 83 and the desired ureas 84–93.^{42–48}

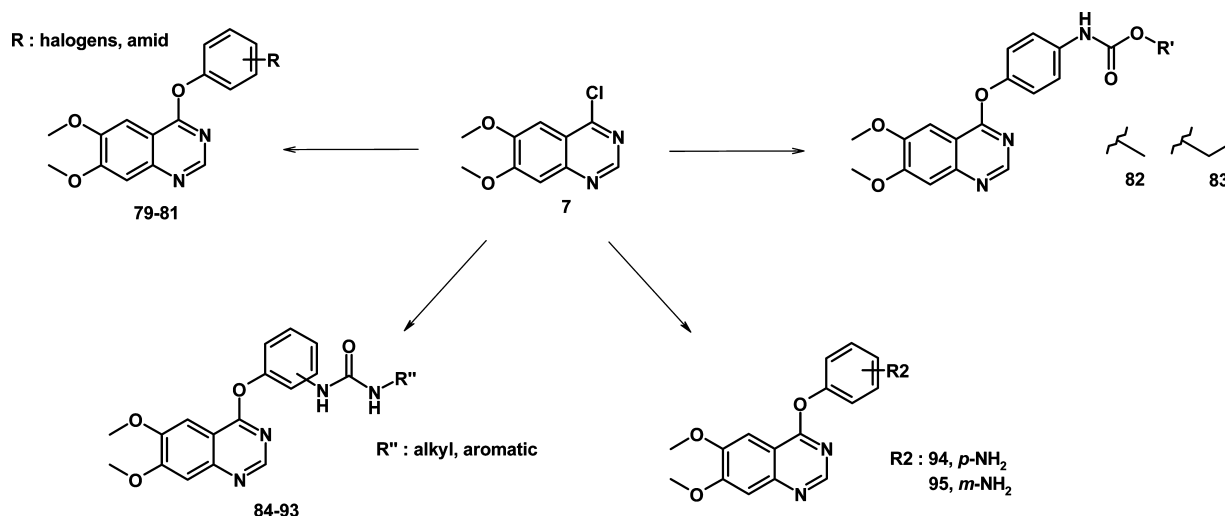
Four series of new quinazolines (series A, B, C, and D), differentiated by having an ether linker at the 6- or 7-position of core and incorporating a donor/acceptor group such as an

acetamide, a carbamic acid ester, or a urea substituted on an arylamino ring, have been designed using structure–activity relationships (Table 1). Suppression of the basic side chain on the quinazoline core confers an increase of cellular and enzymatic inhibitory activity. Our results show that some derivatives of series A and B (6,7-dimethoxyquinazoline) have high activity on EGFR and VEGFR-2 compared to series C and D. Introduction of a urea group led to an increase in VEGFR-2 enzymatic activity but not in EGFR enzymatic activity. Also, replacement of the urea entity by a carbamic acid methyl ester group as in 42 presents a dual EGFR/VEGFR-2 activity. According to investigations, the substitution by halogens on the middle phenyl group of carbamic acid ester and urea derivatives (series A and B) appeared to be a new opportunity to develop a new dual EGFR/VEGFR-2 inhibitor.

Investigation of the SAR around the lead carbamic acid methyl ester 42 revealed a range of potent dual EGFR/VEGFR-2 inhibitors. The substitution by a halogen or methyl on the middle phenyl group of carbamic acid ester increased enzymatic activity. The effect of varying the methoxy groups on the quinazoline core by basic side chain was investigated (series C, D, and E). Our results led to a better affinity against VEGFR-2 and a loss of activity against EGFR.

We have also described the discovery, SAR, and preliminary biological evaluation of a novel series of VEGFR-2-selective tyrosine kinase inhibitors characterized by the replacement of

Scheme 3. Synthesis of (Aryloxy)quinazoline Derivatives



linkers at the 4-position of the quinazoline skeleton by ether (series F and G). The diarylurea of (aryloxy)quinazoline potently inhibited VEGFR-2 at submicromolar concentrations. Molecular modeling established interactions of these compounds with the binding active site. However, their potent activity against VEGFR-2 is not reflected by their antiproliferative activity on cell-based assays due to poor solubility.

According to these results, the substitution by halogens or a methyl group on the middle phenyl group of urea derivatives appears to be a new opportunity to develop a new VEGFR-2-selective inhibitor. Moreover, as a diarylurea moiety is favored for optimal interaction in the active site, others compounds were realized to obtain a better affinity.

These compounds were synthesized according to described procedures in Scheme 4 with 4-chloro-6,7-dimethoxyquinazoline (7) as the starting product. Selective reaction of chloride derivative 7 with 4-amino-3-methylphenol and tetra-*n*-butylammonium bromide in a mixture of methyl ethyl ketone and sodium hydroxide provided the intermediate 96. Condensation of 94 or 96 with the corresponding isocyanate in chloroform afforded the desired ureas 97–102 (Scheme 4).

In Table 2, the diarylurea moiety resulted in excellent kinase inhibition with a nanomolar IC₅₀ value against KDR. There was a selectivity of (aryloxy)quinazoline for this enzyme, against EGFR. Introduction of a methyl group on the phenyl ring (99–102) led to an excellent inhibitory activity against VEGFR-2, in particular for naphthalene derivative 102 (IC₅₀ = 2 nM against VEGFR-2). Substitution of the aromatic group by a bulkier group such as a halide or a naphthalene was tolerated. This enzymatic inhibition was limited by introduction of an electron donor group such as methoxy (87 and 97). These quinazolines were further evaluated in cell-based assays and, unfortunately, were inactive toward different cancer cell lines.

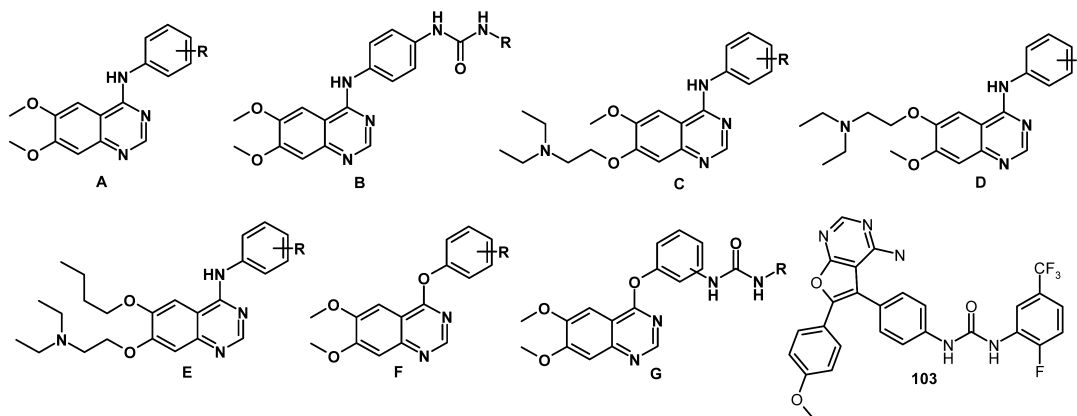
MOLECULAR MODELING

All the calculations have been carried out under the Sybyl 6.9.1 molecular modeling package⁴⁹ running on Silicon Graphics Octane 2 workstations. The ligands were built from the internal fragment library of Sybyl, and their geometries were optimized by the Powell method available in the Maximin2 procedure to a gradient of 0.001 kcal/(mol·Å). The dielectric constant was set to 7.4 to implicitly represent a biological middle, the atomic

charges were attributed by the Gasteiger–Hückel method, and the energy minimization was run with the Tripos force field.⁵⁰

To produce a meaningful conformation for their alignment, the best compounds of the two main substitution patterns (91 and 92) were docked into the VEGFR-2 active site (Table 2). This was carried out by selecting a suitable reference, that is, a structure of the enzyme cocrystallized with an inhibitor structurally related to our compounds. The structure of the protein cocrystallized with a suitable furoprymidinic inhibitor (103) was obtained from the Protein Data Bank (<http://www.pdb.org>)⁵¹ under the entry 1ywn.⁵² The cocrystallized inhibitor and water molecules were removed, and hydrogens were added to the protein, taking care to be as close as possible to the biological protonation state of the residues. The binding mode of the compounds was investigated by a two-step process. They were first docked into the binding site of VEGFR-2 with GOLD 3.2,⁵³ the binding site being defined as a 10 Å sphere around the cocrystallized inhibitor. The multiple conformations generated were then ranked by an in-house consensus scoring based on Goldscore⁵³ and X-Score.⁵⁴ The consistency of the best ranked conformation was visually assessed to make sure it was the most stable binding mode prediction. The molecules were aligned on the best docking conformation of the closer reference compound to give a putative bioactive conformation. The QSAR models were achieved by randomly dividing the pool of 49 compounds into a series of training sets of 33 molecules and corresponding test sets of the 16 remaining molecules (Table 3), following the recommendations by Oprea.⁵⁵ A later batch of 16 more compounds were predicted before their testing as an external test set, therefore assessing the models from the initial 33 compounds on a very large 32-molecule test set. Each training set was employed to generate models using the CoMFA⁵⁶ and CoMSIA⁵⁷ methodologies against the activity of the molecules expressed as pIC₅₀, that is, the opposite of the logarithm of their activity, using the same set of default parameters and the same box for all the models. If they passed a *q*² threshold of 0.3, their external prediction capacity was tested by predicting the values of pIC₅₀ for the corresponding test set compounds, yielding an *r*_{pred}² value. Another relevant parameter is the number of components *N* of the models, showing the relative complexity of the underlying mathematical model. The resulting fields were depicted as the

Table 1. Enzymatic (EGFR/VEGR-2) and Cellular (PC3, Prostate Cancer Cell; HT29, Colon Cancer Cell; MCF-7, Breast Cancer Cell) Results for Quinazoline Derivatives

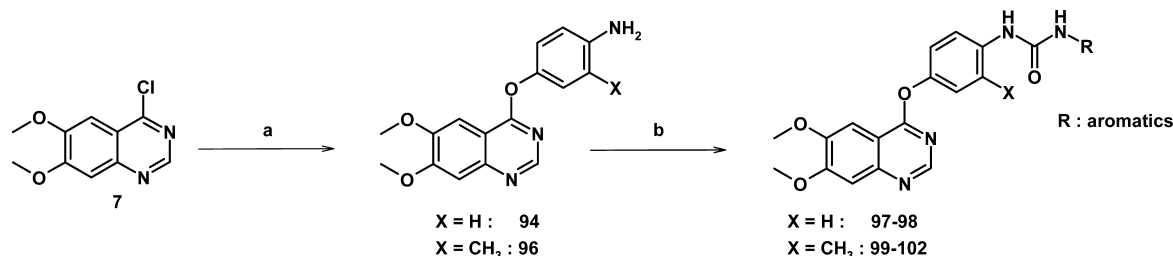


no.	series	compound R	proliferative inhibition, % (or IC ₅₀ , μM) ^{a,d}				
			EGFR IC ₅₀ ^{a,b} μM	VEGFR-2 IC ₅₀ ^{a,c} μM	PC3	HT29	MCF-7
35	A	H	4.30	7.00	9%	0%	7%
36	A	4-Br	3.60	0.80	37%	2%	42%
37	A	3-Cl-4-F	0.38	5.30	6.50 μM	5.70 μM	4.90 μM
38	A	4-Br-2-F	5.70	1.65	1%	0%	31%
39	A	4-(NHCOCH ₂ CH ₃)	>10	7.30	0%	0%	0%
40	A	3-CH ₃ -4-(NHCO(CH ₂) ₂ CH ₃)	>10	4.0	0%	0%	5%
41	A	3-CH ₃ -4-(NHCO(CH ₂) ₃ CH ₃)	>10	6.80	0%	0%	0%
42	A	4-(NHCOOCH ₃)	6.90	5.80	2%	10%	27%
43	A	4-(NHCOOCH ₂ CH ₃)	>10	5.60	12%	16%	6%
44	A	4-(NHCOO(CH ₂) ₂ CH ₃)	7.05	5.00	1%	18%	29%
45	A	4-(NHCOO(CH ₂) ₃ CH ₃)	0.80	6.80	20%	32%	19%
46	A	4-(NHCOOCH(CH ₃) ₂)	4.80	5.05	18%	24%	36%
47	A	3-Cl-4-(NHCOOCH ₃)	6.15	5.05	19%	22%	0%
48	A	3-Cl-4-(NHCOOCH ₂ CH ₃)	1.00	0.50	9.80 μM	30%	0%
49	A	3-Cl-4-(NHCOO(CH ₂) ₂ CH ₃)	1.00	3.30	0%	29%	20%
50	A	3-Cl-4-(NHCOO(CH ₂) ₃ CH ₃)	6.40	4.90	0%	41%	5%
51	A	3-CH ₃ -4-(NHCOOCH ₃)	4.00	0.85	6%	10%	0%
52	A	3-CH ₃ -4-(NHCOOCH ₂ CH ₃)	0.9	0.65	0%	0%	0%
53	A	3-CH ₃ -4-(NHCOO(CH ₂) ₂ CH ₃)	0.9	0.85	6%	18%	0%
54	A	3-CH ₃ -4-(NHCOO(CH ₂) ₃ CH ₃)	7.60	5.20	4%	13%	33%
55	A	3-CH ₃ -4-(NHCOOCH(CH ₃) ₂)	5.80	5.25	3%	2%	30%
56	A	4-Cl-3-(NHCOOCH ₂ CH ₃)	0.90	5.55	13%	4%	39%
57	A	4-CH ₃ -3-(NHCOOCH ₃)	7.20	7.80	0%	0%	12%
58	A	4-CH ₃ -3-(NHCOOCH ₂ CH ₃)	5.00	6.50	0%	0%	1%
59	B	-CH ₂ CH ₃	>10	4.65	0%	0%	6%
60	B	-(CH ₂) ₃ CH ₃	>10	5.80	14%	16%	26%
61	B	phenyl	>10	5.10	35%	5.80 μM	1.50 μM
62	B	3-methoxyphenyl	>10	6.20	43%	45%	7.15 μM
63	B	3-chloro-4-fluorophenyl	>10	4.30	9.40 μM	6.20 μM	7.70 μM
64	C	3-Cl-4-F	9.90	6.90	36%	5.90 μM	26%
65	C	4-Br-2-F	>10	1.00	16%	7.50 μM	10%
66	C	3-Br-4-CH ₃	9.45	6.45	36%	2.55 μM	9.60 μM
67	C	3-Cl-4-(NHCOOCH ₃)	>10	5.20	0%	38%	0%
68	C	3-Cl-4-(NHCOOCH ₂ CH ₃)	>10	3.35	0%	5.45 μM	0%
69	C	3-CH ₃ -4-(NHCOOCH ₃)	>10	6.95	0%	1%	0%
70	C	3-CH ₃ -4-(NHCOOCH ₂ CH ₃)	>10	3.70	0%	11%	0%
71	C	<i>p</i> -(NHCONHCH ₂ CH ₃)	>10	6.60	0%	0%	0%
72	D	4-Br-2-F	9.10	7.45	0%	35%	0%
73	D	3-CH ₃ -4-(NHCOOCH ₂ CH ₃)	>10	7.25	0%	36%	0%
74	E	4-Br-2-F	>10	5.30	31%	3.60 μM	7.70 μM
75	E	3-Cl-4-(NHCOOCH ₃)	>10	7.40	11%	2.55 μM	33%
76	E	3-Cl-4-(NHCOOCH ₂ CH ₃)	9.15	4.80	40%	2.50 μM	7.10 μM
77	E	3-CH ₃ -4-(NHCOOCH ₃)	>10	9.40	0%	6.15 μM	0%
78	E	3-CH ₃ -4-(NHCOOCH ₂ CH ₃)	>10	5.70	0%	5.80 μM	0%

Table 1. continued

no.	series	compound R	EGFR IC ₅₀ ^{a,b} μM	VEGFR-2 IC ₅₀ ^{a,c} μM	proliferative inhibition, % (or IC ₅₀ μM) ^{a,d}		
					PC3	HT29	MCF-7
79	F	3-Cl-4-F	>10	9.80	5%	0%	0%
80	F	4-Br-2-F	5.90	0.60	16%	0%	0%
81	F	3-(NHCOCH ₃)	>10	8.90	0%	0%	5%
82	F	4-(NHCOOCH ₃)	>10	0.70	0%	1%	4%
83	F	4-(NHCOOCH ₂ CH ₃)	>10	0.60	28%	0%	0%
84	G	<i>p</i> -((CH ₂) ₃ CH ₃)	>10	0.40	30%	31%	39%
85	G	<i>p</i> -cyclohexyl	>10	1.00	42%	8%	0%
86	G	<i>p</i> -phenyl	>10	0.06	23%	10%	12%
87	G	<i>p</i> -(4-methoxyphenyl)	>10	0.07	12%	9%	0%
88	G	<i>p</i> -(3-chloro-4-fluorophenyl)	>10	0.04	36%	26%	30%
89	G	<i>p</i> -(2,4-difluorophenyl)	>10	0.09	35%	10%	6.30 μM
90	G	<i>p</i> -(4-bromophenyl)	>10	0.05	2%	13%	10%
91	G	<i>p</i> -(2-naphthyl)	>10	0.03	5%	0%	6.80 μM
92	G	<i>m</i> -phenyl	>10	0.60	19%	7%	0%
93	G	<i>m</i> -(4-methoxyphenyl)	>10	0.60	19%	2%	0%

^aCompounds tested at a concentration of 10 μM. The values are the mean ± SD of at least three independent experiments (SD < 10%). ^bInhibition of EGFR (purified from human carcinoma A431 cells) tyrosine kinase activity. ^cInhibition of VEGFR-2 (recombinant human protein) tyrosine kinase activity. ^dCell proliferation was realized by MTS assay at 10 μM from at least three independent determinations. Higher concentrations were not used to avoid precipitation of the compounds in the culture medium.

Scheme 4^a

^aReagents and conditions: (a) $n\text{Bu}_4\text{N}^+\text{Br}^-$, 2-butanone, 20% NaOH, reflux (84%); (b) isocyanate derivatives, NEt_3 , CHCl_3 , room temperature (35–55%).

zones where the contributions of the fields to the activity were the largest (positive influence, >80%; negative influence, <20%).

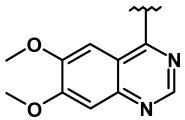
To validate the docking, the cocrystallized ligand **103** was docked using the same procedure as that used for our compounds. The highest scoring conformation is shown in Figure 3 with the cocrystallized conformation. Its rmsd versus the crystallographic conformation is a low 0.436 Å. Moreover, all 30 solutions are closely superimposed and form the same hydrogen bonds with Glu 883 (H on the nitrogens of the urea), with the backbone H of Asp 1044 (carbonyl of the urea), and with the backbone H of Cys 917 (N1 of the pyrimidinic cycle). The only real difference is the position of the terminal methoxy, lying in the plane of the aromatic group in the crystallographic structure and perpendicular to it in the docked conformation. We therefore concluded our docking protocol was sound and assumed the resultant conformation to be representative of the bioactive binding mode of our highest activity compounds.

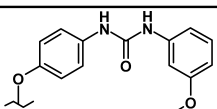
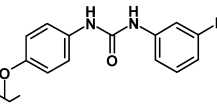
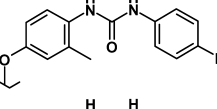
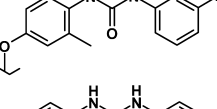
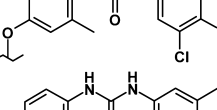
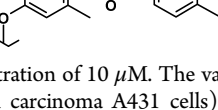
The substitution pattern of the central aromatic tensor of our molecules is either a *para* or a *meta* disubstitution. As easily understood, the *para* pattern gives a conformation closer to that of the cocrystallized compound (Figure 4a), with a good conservation of the spatial position of the molecule from the terminal aromatic group up to the central aromatic tensor. The dimethoxyquinazoline is oriented in the same direction as the central aromatic–urea chain, rather than being upright as in

103. However, the same H bonds are found, with the distal nitrogen of the quinazoline linking with Cys 917 rather than the proximal nitrogen as in the reference compound. The second leader we have docked conserves the position of the important urea and has much the same conformation as its *para* congener. However, the aromatic tensor plane forms an angle of about 140° with **92**. Nonetheless, the distal nitrogen of the dimethoxyquinazoline is at 1.1 Å in the **92** counterpart and is therefore also implied in a H bond with Cys 917 (Figure 4b).

The remaining compounds were aligned on either **91** or **92** following their substitution pattern to yield an alignment. From it, a number of models were created as outlined previously and evaluated for their robustness (N , r^2) and predictive power (q^2 , r_{pred}^2). The five best models are summarized in Table 4. Interestingly, all of them present a number of components N lower than one-fourth of the compounds included in their elaboration, thus meaning they are able to handle the activity values with a fairly simple equation. They are characterized by high r^2 and q^2 above the threshold value of 0.3 we have imposed in the initial selection of the models because this value means a confidence of 95% that the resulting model is not due to a chance correlation.⁵⁸ The major indicative factor of a predictive model is its r_{pred}^2 value. With the exception of the CoMSIA model generated from training set 5, all are above 0.7, heralding the capacity of the models to predict the activity of a previously

Table 2. Enzymatic (EGFR/VEGR-2) and Cellular (PC3, Prostate Cancer Cell; HT29, Colon Cancer Cell; MCF-7, Breast Cancer Cell) Results for New Quinazoline Urea Derivatives



Entry	Compounds R	EGFR (IC ₅₀ , μM) ^{a,b}	VEGFR-2 (IC ₅₀ , μM) ^{a,c}	% Proliferative inhibitory (or IC ₅₀ , μM) ^{a,d}		
				PC3	HT29	MCF-7
97		> 10	0.040	9,40	9,90	9,00
98		> 10	0.006	35%	9.10	9,80
99		> 10	0.040	7%	2%	3%
100		> 10	0.004	25%	36%	30%
101		> 10	0.006	22%	1%	14%
102		> 10	0.002	13%	7%	0%

^aCompounds tested at a concentration of 10 μM. The values are the mean ± SD of at least three independent experiments (SD < 10%). ^bInhibition of EGFR (purified from human carcinoma A431 cells) tyrosine kinase activity. ^cInhibition of VEGFR-2 (recombinant human protein) tyrosine kinase activity. ^dCell proliferation was realized by MTS assay at 10 μM from at least three independent determinations. Higher concentrations were not used to avoid precipitation of the compounds in the culture medium.

unknown compound with a fairly high accuracy of more than 70%. Although it has the highest r_{pred}^2 for both CoMFA and CoMSIA, model 1 is somewhat hampered by its rather low q^2 , indicating it has a poorer internal prediction capacity than the other models. Moreover, it also has a rather high number of components N for its CoMSIA part, indicating that the underlying mathematical model is more complex. Model 2 has the same number of components, but displays improved q^2 and only a very slight decrease in r_{pred}^2 for the CoMFA method. This is correlated to a possible instability in the predictions of the activity of the training set, as the leave-one-out cross-validated r^2 represents the internal predictive power. In essence, at least one of the molecules in the training set could not be predicted from the model derived from the others, resulting in a large prediction error. While fairly attractive, we have not chosen it as our final model due to its relatively large N . The next model fared little better. It is quite correct in terms of predictive power but in our opinion lacks high enough q^2 values, being the second worst model. Moreover, its practical use may be overburdened by the high number of components of the CoMFA part. The two remaining models share some features of interest. First, they display a balanced profile of stability (r^2) and predictivity (q^2 and r_{pred}^2) that can be seen as a proof of their inherent robustness. Second, they have a low number of components, model 4 being better than model 5 in

this aspect. Third, their external predictivity does not appear to be too strongly overestimated. It should be kept in mind that the higher the r_{pred}^2 , the more confident one should be regarding the predictive power of a model. However, evaluation of the predictive capacity is tricky and can very easily lead to a false overconfidence over the reality of the prediction. We were rather suspicious of the r_{pred}^2 nearing 0.90. In the meantime, the goal of the models is to provide biological activities of the compounds prior to their testing as accurately as possible, that is, with the highest r_{pred}^2 possible. We therefore set model 4 as our predictive tool for the last batch of 16 molecules. Interestingly, all the models had a quite close repartition of fields. For the CoMFA models, the steric field is slightly less important than the electrostatic field, in a proportion of about 40/60. For the CoMSIA models, the global trend in field repartition is also well conserved among the models, although the individual percentages between the fields are more varied. Roughly, the steric contribution is about 5%, while the electrostatic fields contribute about 20%. Acceptor fields are fairly unimportant, with a 10% contribution, while hydrophobic and hydrogen bond donor fields are respectively 30% and 35%. This may be relatively well explained when noting that the loss of donor hydrogen bonds around the urea has a larger impact on the binding than the acceptor capacity or size of the molecule, as long as it is able to fit in the pocket. In our study, the large

Table 3. CoMFA- and CoMSIA-Predicted Activities

compound	set	pIC ₅₀	CoMSIA prediction	CoMSIA difference	CoMFA prediction	CoMFA difference
35	test	5.16	5.44	-0.28	5.56	-0.40
36	training	6.12	5.66	0.46	5.54	0.58
37	training	5.27	5.37	-0.10	5.57	-0.30
38	test	5.80	5.81	-0.02	5.73	0.06
39	test	5.14	5.22	-0.08	5.18	-0.04
40	training	5.36	5.54	-0.18	5.65	-0.29
41	training	5.16	5.31	-0.14	5.31	-0.15
42	training	5.24	5.09	0.14	5.22	0.01
43	test	5.25	5.06	0.19	5.01	0.24
44	training	5.30	5.14	0.16	4.82	0.48
45	test	5.16	5.42	-0.25	5.58	-0.42
46	training	5.29	5.13	0.16	5.04	0.25
47	training	5.29	5.25	0.04	5.39	-0.10
49	training	5.48	5.21	0.27	5.18	0.29
50	test	5.31	5.54	-0.23	5.75	-0.44
51	training	6.07	5.49	0.58	5.73	0.34
55	training	5.28	5.37	-0.09	5.43	-0.15
57	test	5.11	4.98	0.13	5.32	-0.22
58	test	5.19	4.82	0.36	5.20	-0.01
59	test	5.33	5.30	0.04	5.39	-0.06
60	test	5.23	5.16	0.07	5.31	-0.08
61	test	5.29	5.65	-0.36	6.17	-0.88
62	training	5.21	5.44	-0.24	5.97	-0.77
63	training	5.37	5.83	-0.46	6.09	-0.72
65	training	6.00	5.83	0.17	5.87	0.13
66	training	5.19	5.52	-0.33	5.07	0.12
67	training	5.28	5.53	-0.25	5.41	-0.13
69	training	5.16	5.43	-0.28	5.64	-0.48
71	training	5.18	4.97	0.21	5.10	0.08
72	test	5.13	5.55	-0.42	5.58	-0.45
74	training	5.28	5.53	-0.26	5.29	-0.01
75	test	5.13	5.14	-0.01	4.69	0.45
77	training	5.03	5.06	-0.03	4.78	0.25
80	training	6.22	6.66	-0.44	6.65	-0.43
81	training	5.05	4.78	0.27	4.96	0.09
82	training	6.17	6.40	-0.23	6.15	0.02
83	training	6.19	6.14	0.05	5.92	0.27
84	training	6.42	6.60	-0.18	6.33	0.09
85	training	6.00	6.49	-0.49	6.44	-0.44
87	training	7.17	6.96	0.21	7.32	-0.15
89	training	7.03	7.13	-0.10	7.32	-0.29
92	test	6.19	4.74	1.45	5.25	0.94
93	training	5.16	4.86	0.30	5.18	-0.03
97	test	7.40	6.81	0.59	7.08	0.32
98	training	8.22	7.84	0.39	7.47	0.75
99	training	7.40	7.53	-0.13	7.75	-0.35
100	training	8.40	8.13	0.27	7.87	0.53
101	training	8.22	7.98	0.24	7.72	0.50
102	test	8.70	7.66	1.03	7.62	1.08

effect of the hydrophobicity is somewhat of a curse, as a high hydrophobicity could have a negative impact on the solubility of the compounds and therefore their cellular effect, while contributing favorably to the binding at a molecular level.

The repartition of the compounds in the training and test sets is shown in Figure 5. All three broad classes of activity (good, from 1 to 2.4; average from 2.5 to 3.4; low above 3.5) are well represented in both sets, with maybe a slight overrepresentation of the good activity compounds in the test set (four of the six compounds of this class). This does not show up prominently in

the predictions of either the CoMSIA (Figure 6) or the CoMFA (Figure 7) model, as there are only two compounds predicted with about 1 log of error by both methods. One of them is compound **102**, which is the most active molecule. Due to the randomness of the repartition in the training and test sets, it fell in the test set and could not be predicted accurately from the compounds in the corresponding training set. By comparison, the second best compound, **91**, was attributed to the training set and is well predicted, therefore showing that the extrapolation from a model should be taken with caution. The second

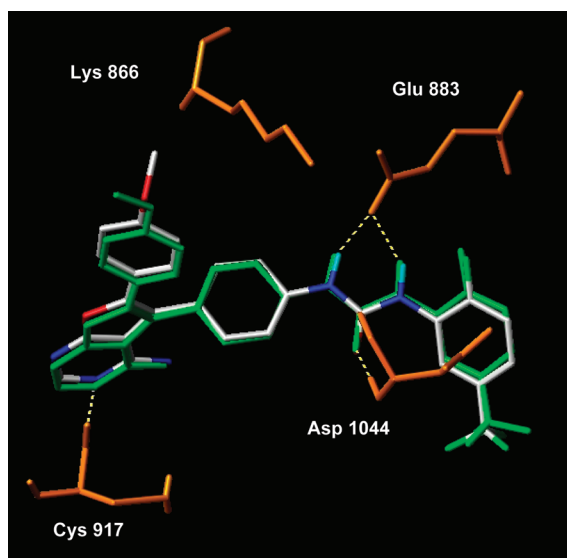


Figure 3. Docking conformation of furo[2,3-*d*]pyrimidine **103** synthesized by Y. Miyazaki⁵² (colored by atom types) compared with the crystallographic conformation (in green).

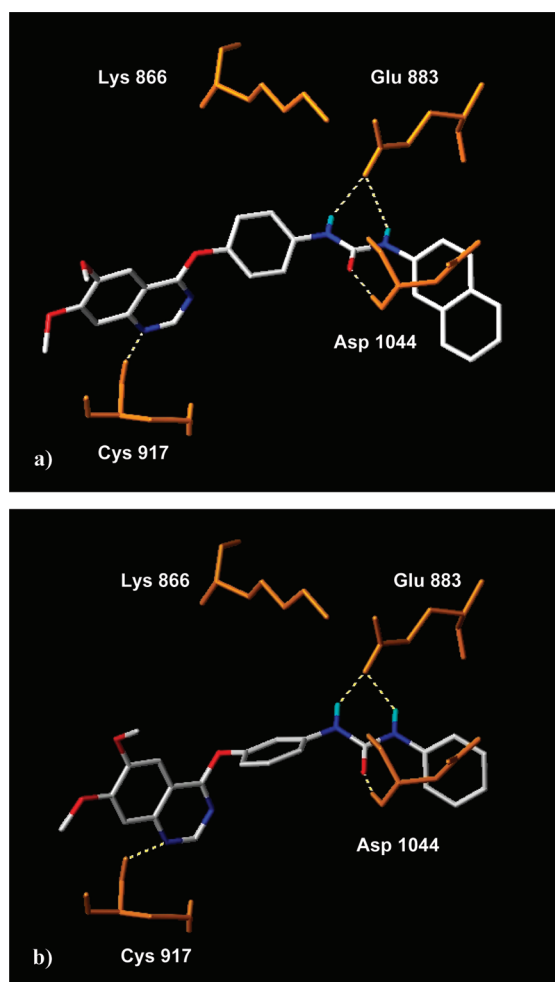


Figure 4. (a) Docking conformation of **91**. (b) Docking of **92**.

mispredicted compound is **92**, which was again classed in the test set. It fared rather poorly in the CoMSIA model, but slightly better in the CoMFA model. In the meantime, high-activity

compounds, such as **98**, **100**, and **101**, were predicted much more accurately, with only compound **98** being missed by more than 0.5 log, and only by the CoMFA method. All of them were used for the training of the model, therefore stressing the possible effect of the underrepresentation of the highest activity class in the training set, rendering the model less able to extrapolate to the best pIC₅₀ values. It should also be noted that compound **69** was not included in the model due to the undetermined nature of its IC₅₀. A series of 16 already synthesized compounds were tested later. We used them to further test the predictive ability of our model by estimating their activity before their testing as an external validation set. The results are presented in Table 5.

Interestingly, the predictions were close enough to the actual values, with 14 compounds out of 16 predicted within 1 log of the experimental values and 11 within 0.5 log. Compound **48** was within 1.2 log, and only compound **79** was really mispredicted, with about 1.5 log of difference for both the CoMFA and CoMSIA models. This could be due to its somewhat shorter length compared to those of most of the other molecules included in the model, as it is a key synthesis intermediary, lacking the urea moiety. With respect to the reduced initial training set, these results implied the model fared fairly well. As a posttesting validation, we tried to create a model trained on all 49 compounds available in the first stage to more accurately predict the remaining 16. The CoMFA and CoMSIA models behaved quite well (Table 6). They are comparable to model 4, with an improved CoMFA r^2 , but a poorer CoMFA q^2 . However, they were not better in the prediction of the second series of compounds (Figure 8). In particular, compound **79** is still mispredicted by about 1.5 log. We therefore have not evaluated any further the development of this model and have reverted to model 4.

The two methods we have employed have the major advantage of providing a visual 3D depiction of the molecular fields around the compounds. We have compared them with the docking of the two lead compounds of our series. The CoMFA fields (Figure 9) give indications of the steric and electrostatic zones of interactions. There are two favorable contours for the steric field. A large contour is next to the aromatic group of the central tensor, where the pocket is widely open. A smaller one is at the other end of the urea, showing the interest of a substitution of an appropriate length on this moiety. The pocket is relatively tightly packed, so the naphthalene of **91** barely fits in this zone, just as the methoxyphenyl of **93**. A totally flexible end group such as the butane of **84** is also of the appropriate length. However, as none of our compounds have a longer chain, we can only guess they should not fit as well in the binding site. The sterically restricted zones complement this first view with a cluster of medium-sized contours around the aromatic tensor, on the side of the benzyl that is opposite that of the favorable zone. This is again in agreement with the binding site geometry, as they correspond to Val 846 and 914, closing this part of the pocket. Interestingly, a large hindrance zone and several smaller zones are placed at the entry of the pocket, indicating that too long groups on the quinazoline side are not useful for the activity and indeed are even unfavorable. This may be linked to the larger moieties replacing the two methoxy groups of the reference molecules, indicating either a loss of activity due to a lowered solubility or just an unfavorable entropic effect of fixing these long chains in a restrictive conformational environment. The electrostatic field is somewhat less informative, with respectively a small and a

Table 4. Statistical Results for the Top Five Models^a

model no.	CoMSIA					CoMFA				
	<i>N</i>	<i>r</i> ²	<i>q</i> ²	<i>r</i> _{pred} ²	fields	<i>N</i>	<i>r</i> ²	<i>q</i> ²	<i>r</i> _{pred} ²	fields
1	5	0.94	0.62	0.86	S, E	3	0.86	0.49	0.88	S, E, H, D, A
2	5	0.94	0.72	0.75	S, E	3	0.89	0.56	0.81	S, E, H, D, A
3	3	0.89	0.63	0.85	S, E	8	0.98	0.58	0.80	S, E, H, D, A
4	4	0.92	0.74	0.73	S, E	3	0.86	0.60	0.75	S, E, H, D, A
5	5	0.95	0.79	0.66	S, E	3	0.86	0.65	0.73	S, E, H, D, A

^aFields used in the models: S (steric), E (electrostatic), H (hydrophobic), D (hydrogen bond donor), A (hydrogen bond acceptor).

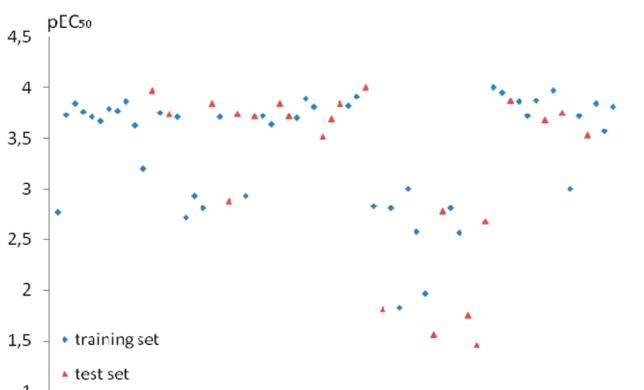


Figure 5. Repartition of the activities of the compounds in the training (blue tilted squares) and test (orange triangles) sets of model 4.

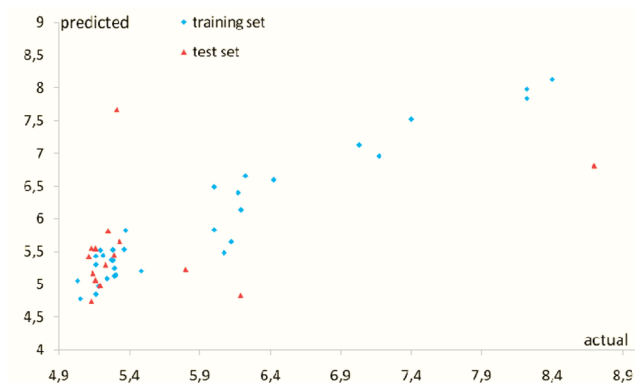


Figure 6. Predictions of CoMSIA model 4 for the training (blue tilted squares) and test (orange triangles) sets.

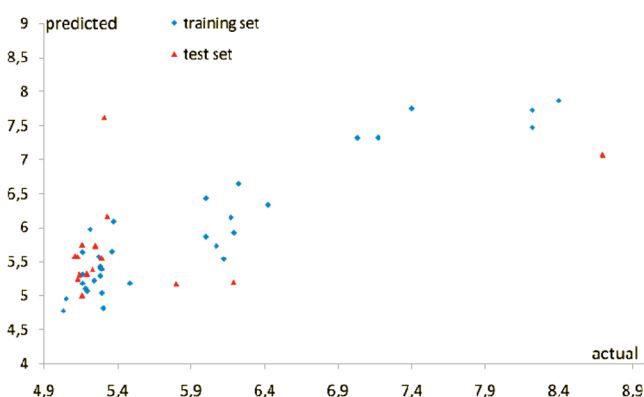


Figure 7. Predictions of CoMFA model 4 for the training (blue tilted squares) and test (orange triangles) sets.

large favorable zone in the middle of the terminal and central aromatic groups of the reference compounds, offering the idea

Table 5. Prediction for the 16 Compounds of the External Validation Set

compound	pIC ₅₀	CoMSIA prediction	CoMSIA difference	CoMFA prediction	CoMFA difference
48	6.28	5.145	1.135	5.314	0.966
52	6.19	5.212	0.978	5.522	0.668
53	6.07	5.115	0.955	5.54	0.53
54	5.28	5.281	-0.001	5.164	0.116
64	5.16	5.478	-0.318	5.476	-0.316
79	5	6.538	-1.538	6.475	-1.475
80	6.22	6.362	-0.142	6.209	0.011
86	7.22	6.903	0.317	7.36	-0.14
88	7.4	6.446	0.954	6.639	0.761
90	7.22	7.099	0.121	7.389	-0.169
91	7.52	7.145	0.375	7.434	0.086
73	5.14	5.087	0.053	5.275	-0.135
76	5.32	5.001	0.319	5.141	0.179
78	5.25	4.996	0.254	5.011	0.239
68	5.47	4.922	0.548	4.834	0.636
70	5.43	5.489	-0.059	5.121	0.309

Table 6. Statistical Results for Model 6

<i>N</i>	CoMSIA			CoMFA		
	<i>r</i> ²	<i>q</i> ²	fields	<i>r</i> ²	<i>q</i> ²	fields
4	0.894	0.753	S, E, H, D, A	0.659	0.870	S, E, H, D, A

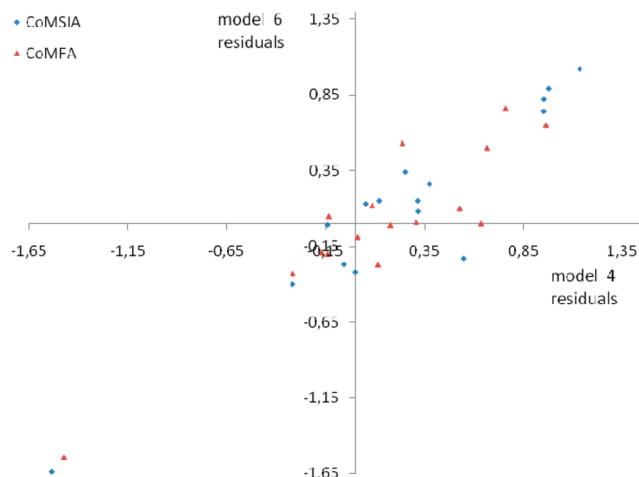


Figure 8. Residuals of the second series of compounds by models 4 and 6 for the CoMFA (orange triangles) and CoMSIA (blue tilted squares) methods.

that these aromatic groups must bear a slightly decreased electronic load. The unfavorable contours and the favorable zone at the methoxy level are nearly useless as they are not related to the protein.

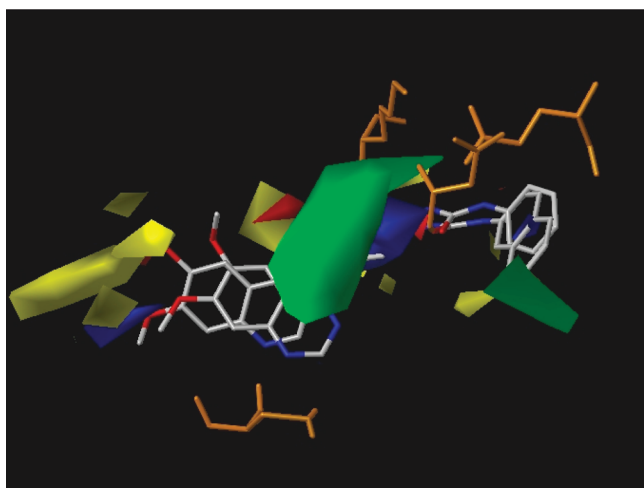


Figure 9. Steric (green, favorable; yellow, unfavorable) and electrostatic (blue, positive charge favorable; red, negative charge favorable) CoMFA fields.

The CoMSIA steric fields (Figure 10a) are larger and more easily interpretable than their CoMFA counterparts, but point to the same trend. Two large favorable contours surround the terminal and central aromatics, clearly hinting to the importance of occupying the right end side of the pocket by a substitution on the urea. The central zone only includes the *meta*-substituted tensor. This may be an artifact related to the larger number of 1,4-substituted molecules having less impact on the variations of the fields. On the contrary, the two unfavorable zones near the methoxy point again to the worsened activity of compounds with longer chains on the oxygens. As previously described, the favorable electrostatic contours (Figure 10a) show the importance of the electronic load of the central aromatic group. However, the urea is surrounded by two zones of major interest. A favorable one is placed next to the carboxy and an unfavorable one next to the distal nitrogen. They may be related to the hydrogen bonding occurring at these positions. The same is true for the favorable zone lying just under the distal nitrogen of the quinazoline. However, the interest of the larger contours around the methoxy is low, due to the aforementioned unfavorable steric effect of long chains in this position and the near to none correlation with residues of the protein. A large hydrophilic contour nearly completely surrounds the aromatic tensor (Figure 10b). This could herald the lowered activity of molecules bearing a substitution of this element other than the straightforward 1,3- or 1,4-disubstitution. However, the smaller hydrophobic region that includes most of the urea is less easy to understand. It might come from the shorter compounds completely missing the urea, for which a hydrophobic substitution is the most common in our study. These compounds are in fact synthesis intermediaries that were tested to assess the effect of the urea. The hydrogen bond donor fields (Figure 10c) display a large favorable contour in front of the nitrogen of the urea. As they are involved in a critical interaction with Glu 883, this contour is in very close agreement with the docking and the previous knowledge of the subject. A medium-sized unfavorable contour appears next to the oxygen of the tensor. Our compounds are built around either a phenoxyquinazoline or an anilinoquinazoline. Therefore, we can conclude easily that the hydrogen capacity of the anilinoquinazoline is not favorable to the activity of the molecules, bringing a fresh insight into the further development

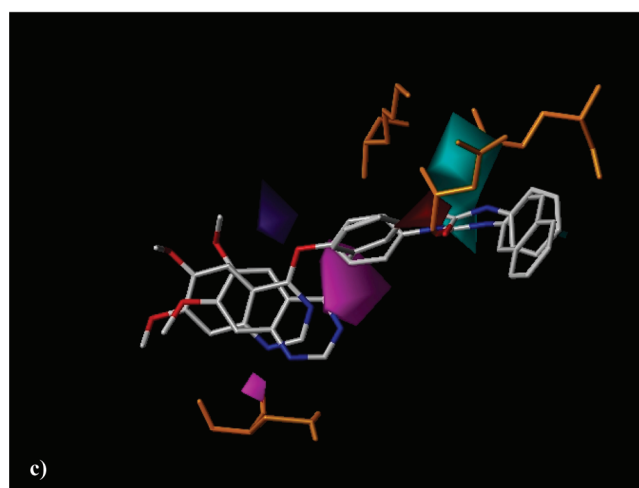
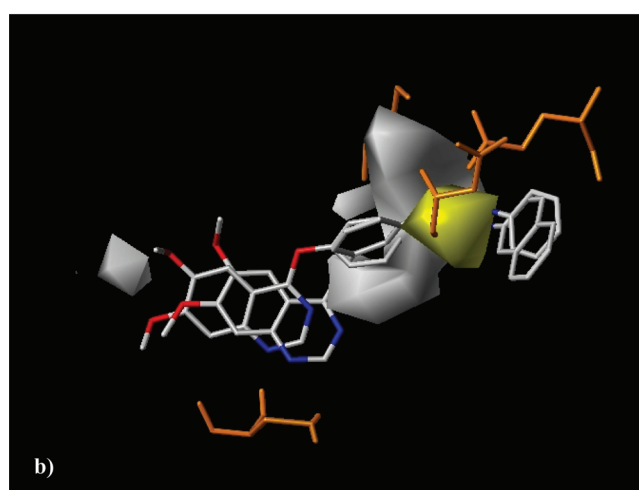
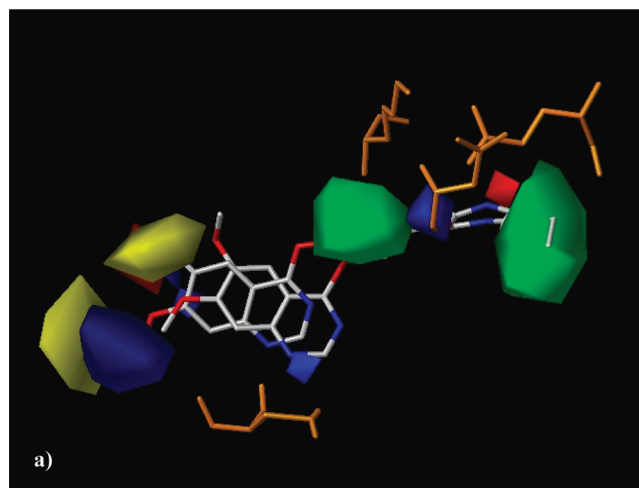
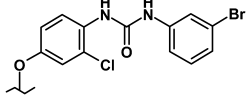
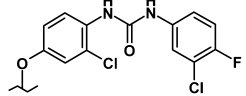
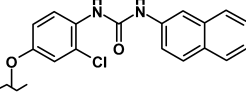
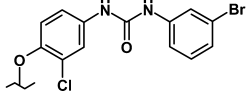
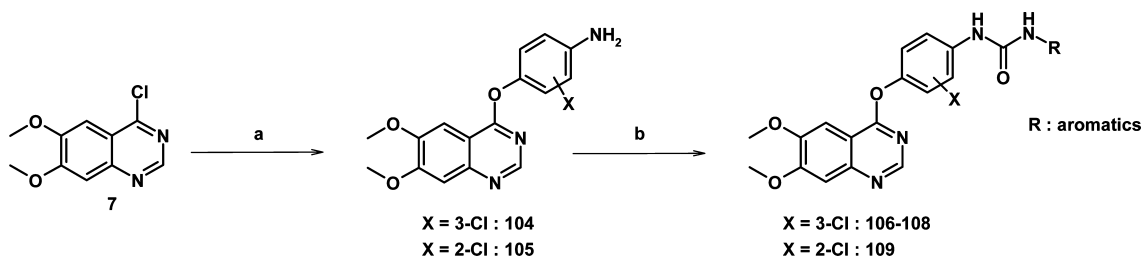


Figure 10. CoMSIA fields of **91** and **92**: (a) steric (green, favorable; yellow, unfavorable) and electrostatic (blue, positive charge favorable; red, negative charge favorable), (b) hydrophobic (yellow, hydrophobic favorable; white, hydrophilic favorable), (c) hydrogen bond donor (cyan, favorable; purple, unfavorable) and acceptor (magenta, favorable; red, unfavorable).

of the series. The acceptor fields are also in very good agreement with the docking. A small favorable contour appears around the Cys 917 backbone hydrogen involved in an interaction with the quinazoline. An unfavorable contour is

Table 7. Prediction for the Four Newly Synthesized Analogues

Entry	Compounds R	pIC_{50}	CoMSIA prediction	CoMSIA error	CoMFA prediction	CoMFA error
106		8.22	7.966	0.254	7.391	0.829
107		8.08	7.886	0.194	7.340	0.74
108		7.39	7.652	-0.262	7.485	-0.095
109		7.70	7.901	-0.202	7.437	0.262

Scheme 5^a

^aReagents and conditions: (a) $nBu_4N^+Br^-$, 2-butanone, 20% NaOH, reflux (40–70%); (b) isocyanate derivatives, NEt_3 , $CHCl_3$, room temperature (10–38%).

displayed above the carbonyl of the urea. This group is engaged in a hydrogen bond with the backbone of Asp 1044, so this result more closely attracted our attention. Upon a closer investigation, this zone prohibits the placement of the carbonyl in an upward position that would hinder its interaction with Asp 1044 rather than clueing toward an unfavorable effect of this interaction. A few compounds of very feeble activity are pointing their carbonyl in this region, with a corresponding loss of the third hydrogen bond of the urea. Lastly, a large favorable contour is drawn around the oxygen of the tensor. It shows that a nitrogen in this position is not the best choice, and reinforces the unfavorable hydrogen donor contour. Taken together, the hydrogen bond fields offer an interesting view of the best scaffold in the series, which should be able to accept a hydrogen from Cys 917 and Asp 1044, give one or two hydrogens to Glu 883, and bear a tensor devoid of a hydrogen donor. All these conclusions are in excellent agreement with the docking, further corroborating the hypothesis of the binding mode we made at the first step of our study.

As they have proved to be quite predictive, these models were employed to imagine new structures and help rank them to prioritize the synthesis of the most promising. We have chosen molecules related to the previous series to keep the synthetic route close to those already described and to preserve the cohesion of the whole series. A number of new structures

were proposed, following these guidelines and the interest of the substitution of the aromatic linker with a hydrophobic moiety, among which the bioisostery of methyl to halogen. Four compounds were chosen for biological evaluation as they were predicted to be the most promising (106–109) (Table 7). These compounds were synthesized according to procedures described in Scheme 5 with the 4-chloro-6,7-dimethoxyquinazolin-2(1H)-one (7) as the starting product. Selective reaction of chloride derivative 7 with 4-amino-3-chlorophenol or 4-amino-2-chlorophenol and tetra-*n*-butylammonium bromide in a mixture of methyl ethyl ketone and sodium hydroxide provided the intermediates 104 and 105. Condensation of 104 or 105 with the corresponding isocyanate in chloroform afforded the desired ureas 106–108 and 109 (Scheme 5).

Most interestingly, none of the compounds were predicted with an error as high as 0.3 log by the CoMSIA model, while the CoMFA model fared somewhat worse, with two underestimated molecules at more than 0.5 log from their experimental value. Moreover, it appeared that the overall ranking of the compounds prior to their synthesis presented no match between the CoMFA ranking and the experimental pIC_{50} . On the other hand, the best and worst compounds of this new series were correctly guessed by the CoMSIA model. In more detail, compound 108, the chlorinated congener of compound 102, was predicted to be close to the latter by the CoMSIA

model, while it was predicted to be noticeably worse by the CoMFA model, which proved to be very precise. This could be due to a less accurate account of the charge repartition on the aromatic center bearing the chlorine by the CoMSIA model. On the basis of methylated compounds **100–102**, we have tried the chlorinated aromatic tensor analogues **106–109**. Relocating the chlorine on this benzene from position 3 to position 2 had the effect of improving the CoMSIA-predicted values, as we expected in part due to the fact that compound **109** is the sole molecule with this substitution pattern. However, it had the reverse effect for CoMFA, most probably due to an overevaluation of the electrostatic effect of the halogen on the charge repartition of the central aromatic group. Experimentally, compound **109** was slightly overpredicted by the CoMSIA model, while compound **106** was largely underestimated by the CoMFA model. Comparing these compounds with their methylated congener, compound **100**, the CoMSIA model accurately predicted the new molecules to be somewhat less good, but rather close to compound **101**, of only slightly lower activity. The effect of this different pattern on the CoMFA prediction is intriguing. Although this model consistently gave not so good predictions for the best compounds of the series, such a high underestimation for compound **106** appears to be related again to the higher electrostatic field contribution in this model. Compound **107**, the chlorinated analogue of compound **101**, suffered from the same drawback, with a serious underestimation from the CoMFA model, while it has been reasonably well predicted by the CoMSIA model. In hindsight, these compounds showed the validity of the models in interpolating to more fully complete the chemical cover of the series but also illustrated the greater robustness of the CoMSIA predictions and the rather low interest of the CoMFA model in predicting better than average activity compounds, maybe due to an overemphasis on the electrostatic field around the central aromatic group.

CONCLUSION

A series of 60 new VEGFR-2 inhibitors have been synthesized and tested on the enzyme. Their activity was evaluated in vitro. In an effort to further develop this series, a QSAR model has been derived from this activity in a two-step process. First, the docking of the most active compound of the two families of molecules has been realized to achieve a putative bioactive conformation. Second, 3D QSAR models employing the CoMFA and CoMSIA methods have been elaborated on the basis of an alignment of the compounds on the putative bioactive conformation of the two reference molecules. The excellent agreement between the docking and the QSAR fields indicates that the binding mode hypothesis is most probably fairly close to the biological binding mode, therefore offering a relevant basis for proposing improvements for the further development of the series. The second major interest of this study is the predictive power of the models, more than their insights into the structural modifications that would enhance the activity of the series, which is too homogeneous to provide an efficient basis for suggesting new scaffolds. This predictive power has been validated on external test sets and further proved on newly synthesized compounds before their biological evaluation. It was employed to propose some new compounds, the most promising of which have been synthesized and tested, with fairly promising results. We plan to further investigate the effect of the modification of the tail of the compounds, lying in a large favorable steric

contour, up to the largest group still able to fit in the binding site, with a combined docking–QSAR–in vitro assay methodology.

EXPERIMENTAL SECTION

Chemistry. Melting points were determined with a Büchi 535 capillary melting point apparatus and are uncorrected. Kieselgel 60 F-254 commercial plates were used for analytical TLC as well as UV light and/or with iodine to follow the course of the reaction. Flash chromatography (FC) was performed with silica gel Kieselgel Si 60, 0.063–0.200 mm (Merck). The structure of each compound was confirmed by IR (Bruker VECTOR 22 instrument) and ¹H NMR (300 MHz, Bruker AC300P spectrometer). Chemical shifts (δ) are reported in parts per million downfield from TMS, *J* values are in hertz, and the splitting patterns are abbreviated as follows: s, singlet; d, doublet; t, triplet; q, quartet; m, multiplet. The purity of the compounds was tested by HPLC separation followed by APCI⁺ (atmospheric pressure chemical ionization) mass spectral detection on an LC–MS system, Thermo Electron Surveyor MSQ, and was >95%.

4-Chloro-6,7-dimethoxyquinazoline (7).⁴³ To a solution of methyl-2-amino-4,5-dimethoxybenzoate (4.0 g, 19.0 mmol) in DMF (40 mL) and methanol (10 mL) were added formamide (76.0 mmol) and sodium methoxide (54.0 mmol). The resulting mixture was refluxed for 16 h. After quenching by water (100 mL), the mixture was neutralized by 1 M HCl solution. The precipitate was collected by filtration, washed with H₂O (30 mL) and Et₂O (30 mL), and dried in vacuo to give quinazolinone **2** as a white solid (82%) which was used directly in the next step. A mixture of **2** (3.0 g, 15.0 mmol) and phosphorus oxychloride (30 mL) was refluxed for 2 h. After removal of the solvent, the residue was dissolved in ice–water (50 mL), and the mixture was neutralized by ammonium hydroxide. The precipitate was collected by filtration and dissolved in CH₂Cl₂ (100 mL). The organic layer was washed with a 1 M solution of K₂CO₃ (3 × 40 mL) and brine (1 × 40 mL) and dried over CaCl₂, and the solvent was removed under reduced pressure. The spectroscopic data for compound **3** are in agreement with those reported in the literature.

4-[(6,7-Dimethoxy-4-quinazolinyloxy)aniline (94).⁴³ A solution of **7** (2.00 g, 8.90 mmol), 4-aminophenol (1.17 g, 10.70 mmol), and tetra-*n*-butylammonium bromide (1.43 g, 4.45 mmol) in methyl ethyl ketone (20 mL) and a 20% solution of NaOH (10 mL) was refluxed for 30 min. After dilution by CHCl₃ (100 mL) and H₂O (20 mL), the organic layer was washed with water and brine and dried over MgSO₄. The solvent was removed under reduced pressure, and then the precipitated solid was collected by filtration and washed with MeOH (15 mL) to give **94** as a white solid (89%). The spectroscopic data for compound **94** are in agreement with those reported in the literature.

3-[(6,7-Dimethoxy-4-quinazolinyloxy)aniline (95).⁴⁸ A solution of **7** (2.00 g, 8.90 mmol), 3-aminophenol (1.17 g, 10.70 mmol), and tetra-*n*-butylammonium bromide (1.43 g, 4.45 mmol) in methyl ethyl ketone (20 mL) and a 20% solution of NaOH (10 mL) was refluxed for 30 min. After dilution by CHCl₃ (100 mL) and H₂O (20 mL), the organic layer was washed with water and brine and dried over MgSO₄. The solvent was removed under reduced pressure, and then the precipitated solid was collected by filtration and washed with MeOH (15 mL) to give **95** as a white solid (93%). The spectroscopic data for compound **95** are in agreement with those reported in the literature.

4-[(6,7-Dimethoxy-4-quinazolinyloxy)-3-methylaniline (96). A solution of **7** (2.00 g, 8.90 mmol), 4-amino-3-methylphenol (1.12 g, 10.70 mmol), and tetra-*n*-butylammonium bromide (1.43 g, 4.45 mmol) in methyl ethyl ketone (20 mL) and a 20% solution of NaOH (10 mL) was refluxed for 30 min. After dilution by CHCl₃ (100 mL) and H₂O (20 mL), the organic layer was washed with water and brine and dried over MgSO₄. The solvent was removed under reduced pressure, and then the precipitated solid was collected by filtration and washed with MeOH (15 mL) to give **96** as a white solid (84%). Mp: 221–223 °C. IR (cm⁻¹): 3384 (NH₂), 1205 (C=C–O), 1075 (C–O–C methoxy). ¹H NMR (DMSO-*d*₆): δ (ppm) 8.51 (s, 1H, ArH), 7.52 (s, 1H, ArH), 7.33 (s, 1H, ArH), 6.57 (d, 1H, *J* = 2.10 Hz, ArH), 6.43 (dd, 1H, *J* = 2.10 and 8.00 Hz, ArH), 6.36 (d, 1H, *J* = 8.01 Hz, ArH), 5.22 (s, 2H, NH₂),

4.02 (s, 3H, OCH₃), 3.98 (s, 3H, OCH₃), 2.15 (s, 3H, CH₃). LC-MS (APCI⁺): *m/z* calcd for C₁₇H₁₇N₃O₃ 312 [(M + H)⁺].

General Procedure for Urea Derivatives 97 and 98. To a stirred solution of **94** (0.20 g, 0.67 mmol) and NEt₃ (0.17 g, 1.68 mmol) in 10 mL of CHCl₃ were added phenyl isocyanate derivatives (0.80 mmol). After 16 h, the residue was filtered off, washed by chloroform (5 mL) and petroleum ether (10 mL), and recrystallized.

***N*-{4-[(6,7-Dimethoxyquinazolin-4-yl)oxy]phenyl}-*N'*-(3-methoxyphenyl)urea (97).** Crystallization from EtOH/H₂O (9S/5) gave pure **97** as a white solid (81%). Mp: 237–239 °C. IR (cm⁻¹): 3214 (NH), 1695 (C=O), 1208 (C=C—O), 1079 (C—O—C methoxy). ¹H NMR (DMSO-*d*₆): δ (ppm) 8.80 (s, 1H, NH), 8.70 (s, 1H, NH), 8.52 (s, 1H, ArH), 7.50–7.60 (m, 3H, ArH), 7.36 (s, 1H, ArH), 7.15–7.25 (m, 4H, ArH), 6.94 (d, *J* = 6.80 Hz, 1H, ArH), 6.55 (d, *J* = 6.80 Hz, 1H, ArH), 4.01 (s, 3H, OCH₃), 3.96 (s, 3H, OCH₃), 3.72 (s, 3H, OCH₃). LC-MS (APCI⁺): *m/z* calcd for C₂₄H₂₂N₄O₅ 447 [(M + H)⁺].

***N*-{3-Bromophenyl}-*N'*-{4-[(6,7-dimethoxyquinazolin-4-yl)oxy]phenyl}urea (98).** Crystallization from acetonitrile gave pure **98** as a white solid (69%). Mp: >250 °C. IR (cm⁻¹): 3214 (NH), 1697 (C=O), 1206 (C=C—O), 1080 (C—O—C methoxy), 1056 (C—Br). ¹H NMR (DMSO-*d*₆): δ (ppm) 8.75 (s, 1H, NH), 8.70 (s, 1H, NH), 8.51 (s, 1H, ArH), 7.50–7.70 (m, 3H, ArH), 7.34 (s, 1H, ArH), 7.15–7.25 (m, 4H, ArH), 6.98 (d, *J* = 7.40 Hz, 1H, ArH), 6.70 (d, *J* = 7.40 Hz, 1H, ArH), 4.01 (s, 3H, OCH₃), 3.97 (s, 3H, OCH₃). LC-MS (APCI⁺): *m/z* calcd for C₂₃H₁₉BrN₄O₄ 495 [(M + H)⁺ for ⁷⁹Br] and 497 [(M + H)⁺ for ⁸¹Br].

General Procedure for Urea Derivatives 99–102. To a stirred solution of **96** (0.20 g, 0.64 mmol) and NEt₃ (0.19 g, 1.60 mmol) in 10 mL of CHCl₃ were added phenyl isocyanate derivatives (0.83 mmol). After 16 h, the residue was filtered off, washed by chloroform (5 mL) and petroleum ether (10 mL), and recrystallized.

***N*-{4-Bromophenyl}-*N'*-{4-[(6,7-dimethoxyquinazolin-4-yl)oxy]-3-methylphenyl}urea (99).** Crystallization from EtOH/H₂O (9S/5) gave pure **99** as a white solid (65%). Mp: >250 °C. IR (cm⁻¹): 3213 (NH), 1695 (C=O), 1206 (C=C—O), 1079 (C—O—C methoxy), 1057 (C—Br). ¹H NMR (DMSO-*d*₆): δ (ppm) 9.02 (s, 1H, NH), 8.52 (s, 1H, NH), 8.01 (s, 1H, ArH), 7.90 (d, *J* = 9.10 Hz, 1H, ArH), 7.57 (s, 1H, ArH), 7.51 (d, *J* = 8.70 Hz, 2H, ArH), 7.39 (s, 1H, ArH), 7.28 (m, 2H, ArH), 7.05–7.15 (m, 3H, ArH), 4.01 (s, 3H, OCH₃), 3.97 (s, 3H, OCH₃), 2.28 (s, 3H, CH₃). LC-MS (APCI⁺): *m/z* calcd for C₂₄H₂₁BrN₄O₄ 509 [(M + H)⁺ for ⁷⁹Br] and 511 [(M + H)⁺ for ⁸¹Br].

***N*-{3-Bromophenyl}-*N'*-{4-[(6,7-dimethoxyquinazolin-4-yl)oxy]-3-methylphenyl}urea (100).** Crystallization from EtOH/H₂O (9S/5) gave pure **100** as a white solid (60%). Mp: >250 °C. IR (cm⁻¹): 3214 (NH), 1695 (C=O), 1206 (C=C—O), 1079 (C—O—C methoxy), 1052 (C—Br). ¹H NMR (DMSO-*d*₆): δ (ppm) 8.85 (s, 1H, NH), 8.75 (s, 1H, NH), 8.10 (s, 1H, ArH), 7.50–7.65 (m, 3H, ArH), 7.35 (s, 1H, ArH), 7.15–7.25 (m, 4H, ArH), 6.95 (m, 1H, ArH), 4.01 (s, 3H, OCH₃), 3.97 (s, 3H, OCH₃), 2.27 (s, 3H, CH₃). LC-MS (APCI⁺): *m/z* calcd for C₂₄H₂₁BrN₄O₄ 509 [(M + H)⁺ for ⁷⁹Br] and 511 [(M + H)⁺ for ⁸¹Br].

***N*-{3-Chloro-4-fluoroanilino}-*N'*-{4-[(6,7-dimethoxyquinazolin-4-yl)oxy]-3-methylphenyl}urea (101).** Crystallization from acetonitrile gave pure **101** as a white solid (75%). Mp: >250 °C. IR (cm⁻¹): 3213 (NH), 1695 (C=O), 1206 (C=C—O), 1079 (C—O—C methoxy), 1057 (C—Cl). ¹H NMR (DMSO-*d*₆): δ (ppm) 9.21 (s, 1H, NH), 8.52 (s, 1H, NH), 8.08 (s, 1H, ArH), 7.80–7.90 (m, 2H, ArH), 7.52 (s, 1H, ArH), 7.30–7.40 (m, 2H, ArH), 7.11 (s, 1H, ArH), 7.08 (d, *J* = 2.30 Hz, 1H, ArH), 4.01 (s, 3H, OCH₃), 3.97 (s, 3H, OCH₃), 2.28 (s, 3H, CH₃). LC-MS (APCI⁺): *m/z* calcd for C₂₄H₂₀ClFN₄O₄ 483 [(M + H)⁺ for ³⁵Cl] and 485 [(M + H)⁺ for ³⁷Cl].

***N*-{4-[(6,7-Dimethoxyquinazolin-4-yl)oxy]-3-methylphenyl}-*N'*-(2-naphthyl)urea (102).** Crystallization from EtOH/H₂O (9S/5) gave pure **102** as a white solid (55%). Mp: >250 °C. IR (cm⁻¹): 3213 (NH), 1697 (C=O), 1206 (C=C—O), 1079 (C—O—C methoxy). ¹H NMR (DMSO-*d*₆): δ (ppm) 9.17 (s, 1H, NH), 8.81 (s, 1H, NH), 8.52 (s, 1H, ArH), 8.15–8.25 (m, 2H, ArH), 7.60–7.80 (m, 2H, ArH), 7.30–7.50 (m, 5H, ArH), 7.13 (s, 1H, ArH), 7.07 (d, *J* = 2.10 Hz, 1H, ArH), 6.95 (d, *J* = 2.40 Hz, 1H, ArH), 4.01 (s, 3H, OCH₃), 3.97

(s, 3H, OCH₃), 2.28 (s, 3H, CH₃). LC-MS (APCI⁺): *m/z* calcd for C₂₈H₂₄N₄O₄ 481 [(M + H)⁺].

4-[(6,7-Dimethoxy-4-quinazolinyloxy]-3-chloroaniline (104). A solution of **7** (2.00 g, 8.90 mmol), 4-amino-3-chlorophenol hydrochloride (1.93 g, 10.70 mmol), and tetra-*n*-butylammonium bromide (1.43 g, 4.45 mmol) in methyl ethyl ketone (20 mL) and a 20% solution of NaOH (10 mL) was refluxed for 30 min. After dilution by CHCl₃ (100 mL) and H₂O (20 mL), the organic layer was washed with water and brine and dried over MgSO₄. The solvent was removed under reduced pressure, and then the precipitated solid was collected by filtration and washed with MeOH (15 mL) to give **104** as a brown solid (70%). Mp: 208–210 °C. IR (cm⁻¹): 3385 (NH₂), 1201 (C=C—O), 1070 (C—O—C methoxy), 1048 (C—Cl). ¹H NMR (DMSO-*d*₆): δ (ppm) 8.53 (s, 1H, ArH), 7.51 (s, 1H, ArH), 7.36 (s, 1H, ArH), 7.22 (d, 1H, *J* = 2.67 Hz, ArH), 6.98 (dd, 1H, *J* = 2.79 and 8.73 Hz, ArH), 6.84 (d, 1H, *J* = 8.76 Hz, ArH), 5.34 (s, 2H, NH₂), 3.97 (s, 3H, OCH₃), 3.95 (s, 3H, OCH₃). LC-MS (APCI⁺): *m/z* calcd for C₁₆H₁₄ClN₃O₃ 331 [(M + H)⁺ for ³⁵Cl] and 333 [(M + H)⁺ for ³⁷Cl].

4-[(6,7-Dimethoxy-4-quinazolinyloxy)-2-chloroaniline (105). A solution of **7** (2.00 g, 8.90 mmol), 4-amino-2-chlorophenol (1.54 g, 10.70 mmol), and tetra-*n*-butylammonium bromide (1.43 g, 4.45 mmol) in methyl ethyl ketone (20 mL) and a 20% solution of NaOH (10 mL) was refluxed for 30 min. After dilution by CHCl₃ (100 mL) and H₂O (20 mL), the organic layer was washed with water and brine and dried over MgSO₄. The solvent was removed under reduced pressure, and then the precipitated solid was collected by filtration and washed with MeOH (15 mL) to give **105** as a brown solid (40%). Mp: >250 °C. IR (cm⁻¹): 3385 (NH₂), 1203 (C=C—O), 1068 (C—O—C methoxy), 1051 (C—Cl). ¹H NMR (DMSO-*d*₆): δ (ppm) 8.50 (s, 1H, ArH), 7.52 (s, 1H, ArH), 7.38 (s, 1H, ArH), 7.05 (d, 1H, *J* = 8.81 Hz, ArH), 6.70 (d, 1H, *J* = 2.62 Hz, ArH), 6.60 (dd, 1H, *J* = 2.32 and 8.80 Hz, ArH), 5.35 (s, 2H, NH₂), 4.00 (s, 3H, OCH₃), 3.95 (s, 3H, OCH₃). LC-MS (APCI⁺): *m/z* calcd for C₁₆H₁₄ClN₃O₃ 331 [(M + H)⁺ for ³⁵Cl] and 333 [(M + H)⁺ for ³⁷Cl].

General Procedure for Urea Derivatives (106–108). To a stirred solution of **104** (0.20 g, 0.60 mmol) and NEt₃ (0.15 g, 1.50 mmol) in 10 mL of CHCl₃ were added phenyl isocyanate derivatives (0.72 mmol). After 16 h at room temperature, the solvent was removed under reduced pressure. The residue was dissolved in AcOEt, washed with a solution of HCl (1 N, 3 × 15 mL), a 10% solution of K₂CO₃ (3 × 15 mL), and brine, and dried over MgSO₄. The solvent was removed under reduced pressure. The residue was purified by FC (CH₂Cl₂/MeOH, 9S/5).

***N*-{3-Bromophenyl}-*N'*-{4-[(6,7-dimethoxyquinazolin-4-yl)oxy]-3-chlorophenyl}urea (106).** Crystallization from EtOH/H₂O (9S/5) gave pure **106** as a white solid (10%). Mp: >250 °C. IR (cm⁻¹): 3210 (NH), 1694 (C=O), 1219 (C—F), 1205 (C=C—O), 1081 (C—O—C methoxy), 1055 (C—Br), 1050 (C—Cl). ¹H NMR (DMSO-*d*₆): δ (ppm) 9.61 (s, 1H, NH), 8.57 (s, 1H, ArH), 8.45 (s, 1H, NH), 8.15 (d, 1H, *J* = 9.60 Hz, ArH), 7.89 (s, 1H, ArH), 7.55–7.58 (m, 2H, ArH), 7.39 (s, 1H, ArH), 7.23–7.32 (m, 3H, ArH), 7.16 (m, 1H, ArH), 3.99 (s, 3H, OCH₃), 3.97 (s, 3H, OCH₃). LC-MS (APCI⁺): *m/z* calcd for C₂₃H₁₈BrClN₄O₄ 529 [(M + H)⁺ for ⁷⁹Br/³⁵Cl], 531 [(M + H)⁺ for ⁷⁹Br/³⁷Cl], 531 [(M + H)⁺ for ⁸¹Br/³⁵Cl], and 533 [(M + H)⁺ for ⁸¹Br/³⁷Cl].

***N*-{3-Chloro-4-fluoroanilino}-*N'*-{4-[(6,7-dimethoxyquinazolin-4-yl)oxy]-3-methylphenyl}urea (107).** Crystallization from EtOH/H₂O (9S/5) gave pure **107** as a white solid (10%). Mp: >250 °C. IR (cm⁻¹): 3211 (NH), 1699 (C=O), 1205 (C=C—O), 1079 (C—O—C methoxy), 1057 (C—Cl). ¹H NMR (DMSO-*d*₆): δ (ppm) 9.89 (s, 1H, NH), 8.68 (s, 1H, ArH), 8.54 (s, 1H, NH), 8.16 (d, 1H, *J* = 9.06 Hz, ArH), 7.83 (dd, *J* = 7.01 and 4.47 Hz, 1H, ArH), 7.59 (s, 1H, ArH), 7.56 (d, 1H, *J* = 2.16 Hz, ArH), 7.42 (s, 1H, ArH), 7.30–7.39 (m, 3H, ArH), 4.01 (s, 3H, OCH₃), 3.98 (s, 3H, OCH₃). LC-MS (APCI⁺): *m/z* calcd for C₂₃H₁₇Cl₂FN₄O₄ 503 [(M + H)⁺ for ³⁵Cl/³⁵Cl], 505 [(M + H)⁺ for ³⁷Cl/³⁵Cl], and 507 [(M + H)⁺ for ³⁷Cl/³⁷Cl].

***N*-{4-[(6,7-Dimethoxyquinazolin-4-yl)oxy]-3-chlorophenyl}-*N'*-(2-naphthyl)urea (108).** Crystallization from EtOH/H₂O (9S/5) gave pure **108** as a white solid (10%). Mp: >250 °C. IR (cm⁻¹): 3213 (NH), 1697 (C=O), 1206 (C=C—O), 1079 (C—O—C methoxy),

1057 (C–Cl). ¹H NMR (DMSO-*d*₆): δ (ppm) 9.62 (s, 1H, NH), 9.33 (s, 1H, ArH), 8.53 (s, 1H, NH), 8.09 (m, 2H, ArH), 7.76–7.84 (m, 4H, ArH), 7.50 (m, 1H, ArH), 7.32–7.48 (m, 3H, ArH), 7.21 (s, 1H, ArH), 6.74 (d, *J* = 8.13 Hz, 1H, ArH), 4.01 (s, 3H, OCH₃), 3.97 (s, 3H, OCH₃), 2.28 (s, 3H, CH₃). LC–MS (APCI⁺): *m/z* calcd for C₂₇H₂₁ClN₄O₄ 501 [(M + H)⁺ for ³⁵Cl/³⁵Cl], 503 [(M + H)⁺ for ³⁷Cl/³⁵Cl], and 505 [(M + H)⁺ for ³⁷Cl/³⁷Cl].

N-(3-Bromophenyl)-*N'*-4-[(6,7-dimethoxyquinazolin-4-yl)oxy]-2-chlorophenylurea (**109**). To a stirred solution of **105** (0.20 g, 0.60 mmol) and NEt₃ (0.15 g, 1.50 mmol) in 10 mL of CHCl₃ was added 3-bromophenyl isocyanate (0.14 g, 0.72 mmol). After 48 h at room temperature, the solvent was removed under reduced pressure. The residue was dissolved in AcOEt, washed with a solution of HCl (1 N, 3 × 15 mL), a 10% solution of K₂CO₃ (3 × 15 mL), and brine, and dried over MgSO₄. The solvent was removed under reduced pressure. The residue was washed by EtOH. Crystallization from EtOH/H₂O (95/5) gave pure **109** as a white solid (38%). Mp: >250 °C. IR (cm⁻¹): 3200 (NH), 1618 (C=O), 1236 (C–F), 1208 (C=C–O), 1137 (C–O–C methoxy), 1048 (C–Br), 1031 (C–Cl). ¹H NMR (DMSO-*d*₆): δ (ppm) 9.05 (s, 1H, NH), 9.01 (s, 1H, NH), 8.54 (s, 1H, ArH), 7.58 (d, 2H, ArH), 7.57 (s, 1H, ArH), 7.40 (m, 3H, ArH), 7.16–7.35 (m, 4H, ArH), 3.99 (s, 3H, OCH₃), 3.98 (s, 3H, OCH₃). LC–MS (APCI⁺): *m/z* calcd for C₂₃H₁₈BrClN₄O₄ 529 [(M + H)⁺ for ⁷⁹Br/³⁵Cl], 531 [(M + H)⁺ for ⁷⁹Br/³⁷Cl], 531 [(M + H)⁺ for ⁸¹Br/³⁵Cl], and 533 [(M + H)⁺ for ⁸¹Br/³⁷Cl].

Cell Culture and Cell Proliferation Assay. Human prostate cancer cells (PC3) and breast cancer cell line MCF7 were grown at 37 °C in a humidified atmosphere containing 5% CO₂ in RPMI-1640 medium (Sigma), minimum essential medium (MEM; Sigma), and Dulbecco's modified Eagle's medium (DMEM; Gibco) supplemented with 10% fetal bovine serum, glutamine (2 mM), penicillin (100 IU/mL), and streptomycin (100 μg/mL). Colon cancer cells (HT29) were grown at 37 °C in a humidified atmosphere containing 5% CO₂ in DMEM + Glutamax-I (Gibco) supplemented with 10% fetal bovine serum, penicillin (100 IU/mL), and streptomycin (100 μg/mL).

In the cell proliferation assay, cells were plated in triplicate on 96-well plates (3000 cells/well) and incubated for 24 h. The cells were then incubated in culture medium that contained various concentrations of tested compounds, each dissolved in less than 0.1% DMSO. After 72 h, cell growth was estimated by the colorimetric MTS test.

In Vitro Kinase Assays. Kinase assays were performed in 96-well plates (Multiscreen Durapore, Millipore) using [γ-³²P]ATP (Amersham Biosciences) and the synthetic polymer poly(Glu4/Tyr) (Sigma Chemicals) as a phosphoacceptor substrate. Tested compounds were dissolved in DMSO. The final concentration of DMSO in the assay solutions was 0.1%, which was shown to have no effect on the kinase activity.

EGFR Tyrosine Kinase Activity. A 20 ng sample of EGFR (purified from human carcinoma A431 cells, Sigma Chemicals) was incubated for 1 h at 28 °C using various concentrations of tested compounds in kinase buffer (HEPES, 50 mM, pH 7.5, BSA, 0.1 mg/mL, MnCl₂, 10 mM, MgCl₂, 5 mM, Na₃VO₄, 100 μM, DTT, 0.5 mM, poly(Glu4/Tyr), 250 μg/mL, ATP, 5 μM, [γ-³²P]ATP, 0.5 μCi).

VEGFR-2 Tyrosine Kinase Activity. A 10 ng sample of VEGFR-2 (recombinant human protein, Invitrogen) was incubated for 1 h at 28 °C using various concentrations of tested compounds in kinase buffer (Tris, 50 mM, pH 7.5, BSA, 25 μg/mL, MnCl₂, 1.5 mM, MgCl₂, 10 mM, DTT, 2.5 mM, Na₃VO₄, 100 μM, β-glycerophosphate, 5 mM, poly(Glu4/Tyr), 250 μg/mL, ATP, 5 μM, [γ-³²P]ATP, 0.5 μCi).

The reaction was stopped by adding 20 μL of trichloroacetic acid, 100%. The wells were screened and washed 10 times with trichloroacetic acid, 10%. The plates were counted in a Top Count for 1 min/well.

AUTHOR INFORMATION

Corresponding Author

*Phone: +33 (0)3 20 96 40 40. Fax: +33 (0)3 20 96 49 06. E-mail: amaury.farce-2@univ-lille2.fr.

ACKNOWLEDGMENTS

Kinase assays were realized on the Binding-Platform of ICPAL, Université Lille 2, supported by PRIM (Pôle de Recherche Interdisciplinaire pour le Médicament). We thank the LaRMNS, RMN Laboratory, Faculty of Pharmacy.

ABBREVIATIONS USED

ATP, adenosine 5'-triphosphate; DMF, *N,N*-dimethylformamide; DMSO, dimethyl sulfoxide; EtOAc, ethyl acetate; EtOH, ethanol; FC, flash chromatography; MeOH, methanol; rt, room temperature

REFERENCES

- (1) Barton, J.; Blackledge, G.; Wakeling, A. Growth factor and their receptors: new targets for prostate cancer therapy. *Urology* **2001**, *58*, 114–122.
- (2) Cohen, P. The role of protein phosphorylation in human health and disease. *Eur. J. Biochem.* **2001**, *268*, 5001–5010.
- (3) Levitzki, A. Protein kinase inhibitors as a therapeutic modality. *Acc. Chem. Res.* **2003**, *36*, 462–469.
- (4) Cohen, P. Protein kinases—the major drug targets of the twenty-first century? *Nat. Rev. Drug Discovery* **2002**, *1*, 309–315.
- (5) Zwick, E.; Bange, J.; Ullrich, A. Receptor tyrosine kinase as targets for anticancer drugs. *Trends Mol. Med.* **2002**, *8*, 17–22.
- (6) Traxler, P.; Bold, G.; Buchdunger, E.; Caravatti, G.; Furet, P.; Manley, P.; O'Reilly, T.; Wood, J.; Zimmermann, J. Tyrosine kinase inhibitors: from rational design to clinical trials. *Med. Res. Rev.* **2001**, *21*, 499–512.
- (7) Traxler, P. Tyrosine kinases as targets in cancer therapy—successes and failures. *Exp. Opin. Ther. Targets* **2001**, *21*, 499–512.
- (8) Carmeliet, P. Angiogenesis in health and disease. *Nat. Med.* **2003**, *9*, 653–660.
- (9) Otrrock, Z. K.; Makarem, J. A.; Shamseddine, A. I. Vascular endothelial growth factor family of ligands and receptors: reviews. *Blood Cells, Mol. Dis.* **2007**, *38*, 258–268.
- (10) Bishop-Bailey, D. Tumour vascularisation: a druggable target. *Curr. Opin. Pharmacol.* **2009**, *9*, 96–101.
- (11) Hida, K.; Hida, Y.; Shindoh, M. Understanding tumor endothelial cell abnormalities to develop ideal anti-angiogenic therapies. *Cancer Sci.* **2008**, *99*, 459–466.
- (12) Otrrock, Z. K.; Mahfouz, R. A. R.; Makarem, J. A.; Shamseddine, A. I. Understanding the biology of angiogenesis: review of the most important molecular mechanisms. *Blood Cells, Mol. Dis.* **2007**, *39*, 212–220.
- (13) Senger, D. R.; Van de Water, L.; Brown, L. F.; Nagy, J. A.; Yeo, K. T.; Yeo, T. K.; Berse, B.; Jackman, R. W.; Dvorak, A. M.; Dvorak, H. F. Vascular permeability factor (VPF, VEGF) in tumor biology. *Cancer Metastasis Rev.* **1993**, *12*, 303–324.
- (14) Roy, H.; Bhardwaj, S.; Ylä-Herttua, S. Biology of vascular endothelial growth factors. *FEBS Lett.* **2006**, *580*, 2879–2887.
- (15) Huang, Z.; Bao, S. D. Roles of main pro- and anti-angiogenic factors in tumor angiogenesis. *World J. Gastroenterol.* **2004**, *4*, 463–470.
- (16) Gleadle, J. M.; Ratcliffe, P. J. Hypoxia and the regulation of gene expression. *Mol. Med. Today* **1998**, *4*, 122–129.
- (17) Ferrara, N.; Davis-Smyth, T. The biology of vascular endothelial growth factor. *Endocr. Rev.* **1997**, *18*, 4–25.
- (18) Roskoski, R. Jr. Vascular endothelial growth factor (VEGF) signaling in tumor progression. *Crit. Rev. Oncol. Hematol.* **2007**, *62*, 179–213.
- (19) Roskoski, R. Jr. VEGF receptor protein-tyrosine kinases: structure and regulation. *Biochem. Biophys. Res. Commun.* **2008**, *375*, 287–291.
- (20) Shibuya, M.; Claesson-Welsh, L. Signal transduction by VEGF receptors in regulation of angiogenesis and lymphangiogenesis. *Exp. Cell Res.* **2006**, *312*, 549–560.
- (21) Rahimi, N. Vascular endothelial growth factor receptors: molecular mechanisms of activation and therapeutic potentials. *Exp. Eye Res.* **2006**, *83*, 1005–1016.

- (22) Schlessinger, J. Cell signaling by receptor tyrosine kinases. *Cell* **2000**, *103*, 211–225.
- (23) Hunter, T. Tyrosine phosphorylation: thirty years and counting. *Curr. Opin. Cell Biol.* **2009**, *21*, 140–146.
- (24) Gibson, K. H.; Grundy, W.; Godfrey, A.; Woodburn, J. R.; Ashton, S. E.; Curry, B. J.; Scarlett, L.; Barker, A. J.; Brown, D. S. Epidermal growth factor receptor tyrosine kinase: structure-activity relationships and antitumor activity of novel quinazolines. *Bioorg. Med. Chem. Lett.* **1997**, *7*, 2723–2728.
- (25) Kohno, M.; Pouyssegur, J. Targeting the Erk signalling pathway in cancer therapy. *Ann. Med.* **2006**, *38*, 200–211.
- (26) Djordjevic, S.; Driscoll, P. C. Structural insight into substrate specificity and regulatory mechanisms of phosphoinositide 3-kinases. *Trends Biochem. Sci.* **2002**, *27*, 445–452.
- (27) Gourley, M.; Williamson, J. S. Angiogenesis: new targets for the development of anticancer chemotherapies. *Curr. Pharm. Des.* **2000**, *6*, 417–439.
- (28) Brunella, C.; Costanza, E. Possible novel targets for therapeutic angiogenesis. *Curr. Opin. Pharmacol.* **2009**, *9*, 102–108.
- (29) Raffetto, J. D.; Khalil, R. A. Matrix metalloproteinases and their inhibitors in vascular remodeling and vascular disease. *Biochem. Pharmacol.* **2008**, *75*, 346–359.
- (30) Hida, K.; Hida, Y.; Shindoh, M. Understanding tumor endothelial cell abnormalities to develop ideal anti-angiogenic therapies. *Cancer Sci.* **2008**, *99*, 459–466.
- (31) Masood, R.; Kundra, A.; Zhu, S.; Xia, G.; Scalia, P.; Smith, D. L.; Gill, P. S. Malignant mesothelioma growth inhibition by agents that target the VEGF and VEGF-C autocrine loops. *Int. J. Cancer* **2003**, *104*, 603–610.
- (32) Booy, E. P.; Johar, D.; Maddika, S.; Pirzada, H.; Sahib, M. M.; Gehrke, I.; Loewen, S.; Louis, S. F.; Kadkhoda, K.; Mowat, M.; Los, M. Monoclonal and bispecific antibodies as novel therapeutics. *Arch. Immunol. Ther. Exp.* **2006**, *54*, 85–101.
- (33) Ferrara, N.; Hillan, K. J.; Novotny, W. Bevacizumab (Avastin), a humanized anti-VEGF monoclonal antibody for cancer therapy. *Biochem. Biophys. Res. Commun.* **2005**, *333*, 328–335.
- (34) Scanga, A.; Kowdley, K. Sorafenib: a glimmer of hope for unresectable hepatocellular carcinoma? *Hepatology* **2009**, *49*, 332–334.
- (35) Escudier, B.; Eisen, T.; Stadler, W. M.; Szczylik, C.; Oudard, S.; Siebels, M.; Negrier, S.; Chevreaux, C.; Solska, E.; Desai, A. A.; Rolland, F.; Demkow, T.; Hutson, T. E.; Gore, M.; Freeman, S.; Schwartz, B.; Shan, M.; Simantov, R.; Bukowski, R. M. Sorafenib in advanced clear-cell renal-cell carcinoma. *N. Eng. J. Med.* **2009**, *49*, 332–334.
- (36) Motzer, R. J.; Michaelson, M. D.; Redman, B. G.; Hudes, G. R.; Wilding, G.; Figlin, R. A.; Ginsberg, M. S.; Kim, S. T.; Baum, C. M.; DePrimo, S. E.; Li, J. Z.; Bello, C. L.; Theuer, C. P.; George, D. J.; Rini, B. I. Activity of SU11248, a multitargeted inhibitor of vascular endothelial growth factor receptor and platelet-derived growth factor receptor, in patients with metastatic renal cell carcinoma. *J. Clin. Oncol.* **2006**, *24*, 16–24.
- (37) Ryan, A. J.; Wedge, S. R. ZD6474—a novel inhibitor of VEGFR and EGFR tyrosine kinase. *Br. J. Cancer* **2005**, *92*, S6–S13.
- (38) Ciardiello, F.; Bianco, R.; Caputo, R.; Caputo, R.; Damiano, V.; Troiani, T.; Melisi, D.; De Vita, F.; De Placido, S.; Bianco, A. R.; Tortora, G. Antitumor activity of ZD6474, a vascular endothelial growth factor receptor tyrosine kinase inhibitor, in human cancer cells with acquired resistance to anti-epidermal growth factor receptor therapy. *Clin. Cancer Res.* **2004**, *10*, 784–793.
- (39) Morabito, A.; Piccirillo, M. C.; Falasconi, F.; De Feo, G.; Del Giudice, A.; Bryce, J.; Di Maio, M.; De Maio, E.; Normanno, N.; Perrone, F. Vandetanib (ZD6474), a dual inhibitor of vascular endothelial growth factor receptor (VEGFR) and epidermal growth factor receptor (EGFR) tyrosine kinases: current status and future directions. *Oncologist* **2009**, *14*, 378–390.
- (40) Garofalo, A.; Goossens, L.; Lemoine, A.; Farce, A.; Arlot, Y.; Depreux, P. Quinazoline-urea, new protein kinase inhibitors in treatment of prostate cancer. *J. Enzyme Inhib. Med. Chem.* **2010**, *25*, 158–171. Pandey, A.; Volkots, D. L.; Seroogy, J. M.; Rose, J. W.; Yu, J. C.; Lambing, J. L.; Hutchaleelaha, A.; Hollenbach, S. J.; Abe, K.; Giese, N. A.; Scarborough, R. M. Identification of orally active, potent, and selective 4-piperazinylquinazolines as antagonists of the platelet-derived growth factor receptor tyrosine kinase family. *J. Med. Chem.* **2002**, *45*, 3772–3793.
- (41) Garofalo, A.; Goossens, L.; Lemoine, A.; Ravez, P.; Six, P.; Howsam, M.; Farce, A.; Depreux, P. (4-(6,7-Disubstituted quinazolin-4-ylamino)phenyl) carbamic acid ester: a novel series of dual EGFR/VEGFR-2 receptor tyrosine kinase inhibitors. *MedChemComm* **2011**, *2*, 65–72.
- (42) Garofalo, A.; Goossens, L.; Farce, A.; Lemoine, A.; Ravez, P.; Six, P.; Depreux, P. Impact of aryloxy-linked quinazolines: a novel series of selective VEGFR-2 receptor tyrosine kinase inhibitors. *Bioorg. Med. Chem. Lett.* **2011**, *21*, 2106–2112.
- (43) Furuta, T.; Sakai, T.; Senga, T.; Osawa, T.; Kubo, K.; Shimizu, T.; Suzuki, R.; Yoshino, T.; Endo, M.; Miwa, A. Identification of potent and selective inhibitors of PDGF Receptor autophosphorylation. *J. Med. Chem.* **2006**, *49*, 2186–2192.
- (44) Desroses, M.; Laconde, G.; Depreux, P.; Hénichart, J. P. Synthesis of unsymmetrical dialkoxy quinazolines. *Org. Prep. Proced. Int.* **2004**, *36*, 445–452.
- (45) Telliez, A.; Desroses, M.; Pommery, N.; Briand, O.; Farce, A.; Laconde, G.; Lemoine, A.; Depreux, P.; Hénichart, J. P. Derivatives of Iressa, a specific epidermal growth factor receptor inhibitor, are powerful apoptosis inducers in PC3 prostatic cancer cells. *ChemMedChem* **2007**, *2*, 318–332.
- (46) Garofalo, A.; Goossens, L.; Lebegue, N.; Depreux, P. A novel and efficient one-pot synthesis of (aminophenyl)carbamic acid ester. *Synth. Commun.* **2011**, *41*, 2007–2016.
- (47) Elliott, R. D.; Thomas, H. J.; Shaddix, S. C.; Adamson, D. J.; Brockman, R. W.; Riordan, J. M.; Montgomery, J. A. Nitrosoureido nucleosides as potential inhibitors of nucleotide biosynthesis. *J. Med. Chem.* **1988**, *31*, 250–254.
- (48) Garofalo, A.; Goossens, L.; Baldyrou, B.; Lemoine, A.; Ravez, S.; Six, P.; David-Cordonnier, M. H.; Bonte, J. P.; Depreux, P.; Lansiaux, A.; Goossens, J. F. Design, synthesis and DNA-binding of N-alkyl(anilino)-quinazoline derivatives. *J. Med. Chem.* **2010**, *53*, 8089–8103.
- (49) SYBYL 6.9.1; Tripos Inc.: St. Louis, MO, 2003.
- (50) Clark, M.; Cramer, R. D. III; van Opdenbosch, N. Validation of the general purpose Tripos 5.2 force field. *J. Comput. Chem.* **1989**, *10*, 982–1012.
- (51) Berman, H. M.; Westbrook, J.; Feng, Z.; Gary, G.; Bhat, T. N.; Weissig, H.; Shindyalov, I. N.; Bourne, P. E. The Protein Data Bank. *Nucleic Acids Res.* **2000**, *28*, 235–242.
- (52) Miyazaki, Y.; Matsunaga, S.; Tang, J.; Maeda, Y.; Nakano, M.; Philippe, R. J.; Shibahara, M.; Liu, W.; Sato, H.; Wang, L.; Nolte, R. T. Novel 4-amino-furo[2,3-d]pyrimidines as Tie-2 and VEGFR2 dual inhibitors. *Bioorg. Med. Chem. Lett.* **2005**, *15*, 2203–2207.
- (53) Jones, G.; Willett, P.; Glen, R. C.; Leach, A. R.; Taylor, R. Development and validation of a genetic algorithm for flexible docking. *J. Mol. Biol.* **1997**, *267*, 727–748.
- (54) Wang, R.; Lai, L.; Wang, S. J. Further development and validation of empirical scoring functions for structure-based binding affinity prediction. *J. Comput.-Aided Mol. Des.* **2002**, *16*, 11–26.
- (55) Oprea, T. I.; Waller, C. L.; Marshall, G. R. Three-dimensional quantitative structure-activity relationship of human immunodeficiency virus (I) protease inhibitors. 2. Predictive power using limited exploration of alternate binding modes. *J. Med. Chem.* **1994**, *37*, 2206–2215.
- (56) Cramer, R. D. III; Patterson, D. E.; Bunce, J. D. Comparative molecular field analysis (CoMFA). 1. Effect of shape on binding of steroids to carrier proteins. *J. Am. Chem. Soc.* **1988**, *110*, 5959–5967.
- (57) Klebe, G.; Abraham, U.; Mietzner, T. Molecular similarity indices in a comparative analysis (CoMSIA) of drug molecules to correlate and predict their biological activity. *J. Med. Chem.* **1994**, *37*, 4130–4146.
- (58) Clark, M.; Cramer, R. D. III. The probability of chance correlation using partial least squares (PLS). *Quant. Struct.-Act. Relat.* **1993**, *12*, 137–145.